Mitochondrial ETF insufficiency drives neoplastic growth by selectively optimizing cancer bioenergetics

David Papadopoli[1,2*], Ranveer Palia[1,3], Predrag Jovanovic[1,3], Sébastien Tabariès[4], Emma Ciccolini[1,3], Valerie Sabourin[1], Sebastian Igelmann[5], Shannon McLaughlan[6], Lesley Zhan[6], HaEun Kim[3], Nabila Chekkal[6], Krzysztof J. Szkop[7], Thierry Bertomeu[8], Jibin Zeng[1], Julia Vassalakis[9], Farzaneh Afzali[9], Slim Mzoughi[10], Ernesto Guccione[10], Mike Tyers[11], Daina Avizonis[4,12], Ola Larsson[7], Lynne-Marie Postovit[9], Sergej Djuranovic[13,14], Josie Ursini-Siegel[1,2,3,6], Peter M. Siegel[3,4,6], Michael Pollak[1,2,3*], Ivan Topisirovic[6*]

[1]Lady Davis Institute, SMBD JGH, McGill University, Montréal, QC H3T 1E2, Canada.

[2]Gerald Bronfman Department of Oncology, McGill University, Montréal, QC H3A 0G4, Canada.

[3]Department of Experimental Medicine, McGill University, Montréal, QC H3A 0G4, Canada.

[4]Rosalind and Morris Goodman Cancer Institute, McGill University, Montréal, QC H3A 1A3, Canada

[5]VIB Center for Cancer Biology, Department of Oncology, KU Leuven and Leuven Cancer Institute (LKI), Herestraat 49, 3000 Leuven, Belgium.

[6]Department of Biochemistry, McGill University, Montréal, QC H3A 0G4, Canada.

[7]Department of Oncology-Pathology, Science for Life Laboratory, Karolinska Institute, 171 77, Stockholm, Sweden.

[8]Institute for Research in Immunology and Cancer, Université de Montréal, Montréal, QC H3T 1J4, Canada.

23 [9]Department of Biomedical and Molecular Sciences, Queen's University, Kingston, ON K7L 3N6,
24 Canada.
25 [10]Center of OncoGenomics and Innovative Therapeutics (COGIT), Department of Oncological
26 Sciences, Tisch Cancer Institute, Icahn School of Medicine at Mount Sinai, New York, NY, 10029
27 United States.
28 [11]Program in Molecular Medicine, The Hospital for Sick Children, Toronto, ON M5G 0A4,
29 Canada. Department of Molecular Genetics, University of Toronto, Toronto, ON M5S 1A8,
30 Canada.
31 [12]Metabolomics Innovation Resource, McGill University, Montréal, QC, Canada.
32 [13]Department of Cell Biology and Physiology, Washington University School of Medicine, St.
33 Louis, MO 63110, United States.
34 [14]Department of Molecular Biology, Cell Biology and Biochemistry, Brown University,
35 Providence, RI 02903, United States.
36 [*]Correspondence david.papadopoli@mail.mcgill.ca (D.P), michael.pollak@mcgill.ca (M.P.),
37 ivan.topisirovic@mcgill.ca (I.T.)
38
39 **Keywords**: Electron transfer flavoprotein dehydrogenase (ETFDH), cancer metabolism, mRNA
40 translation, mechanistic target of rapamycin (mTOR), 4E-binding protein 1 (4E-BP1).
41
42
43
44
45

Abstract

Mitochondrial electron transport flavoprotein (ETF) insufficiency causes metabolic diseases known as a multiple acyl-CoA dehydrogenase deficiency (MADD). In contrast to muscle, ETFDH is a non-essential gene in acute lymphoblastic leukemia NALM-6 cells, and its expression is reduced across human cancers. ETF insufficiency caused by decreased ETFDH expression limits flexibility of OXPHOS fuel utilization but paradoxically increases cancer cell bioenergetics and accelerates neoplastic growth by activation of the mTORC1/BCL-6/4E-BP1 axis. Collectively, these findings reveal that while ETF insufficiency is rare and has detrimental effects in non-malignant tissues, it is common in neoplasia, where ETFDH downregulation leads to bioenergetic and signaling reprogramming that accelerate neoplastic growth.

69 **Main**

70 The mitochondrial electron transport chain (ETC) transfers electrons from reducing
71 equivalents (NADH and $FADH_2$) towards complexes I/II, or from peripheral metabolic enzymes
72 that reduce coenzyme Q (ubiquinone, Q) to ubiquinol (QH_2) [1]. The electron transfer flavoproteins
73 (ETFA and ETFB) accept electrons generated by the catabolism of branched-chain amino acids
74 and fatty acids [2-4]. ETFs interact with ETF dehydrogenase (ETFDH or ETF-ubiquinone
75 oxidoreductase) [5], which controls electron flow towards complex III (Supplementary Fig.1A).
76 Loss-of-function mutations in ETF/ETFDH occur in metabolic diseases known as multiple acyl-
77 CoA dehydrogenase deficiency (MADD) [6,7]. ETFDH is also essential for complex III activity in
78 skeletal muscle [8]. Surprisingly, we observed that in contrast to muscle, ETFDH is one of the most
79 non-essential metabolic genes in cancer cells. Paradoxically, ETFDH downregulation leads to
80 enhanced mitochondrial biogenesis and increased bioenergetic capacity of cancer cells. ETF
81 insufficiency resulting from reduction in ETFDH levels triggers a tradeoff favored by cancer cells,
82 whereby reduced flexibility in fuel utilization for oxidative phosphorylation is offset by signaling
83 from mitochondria to mTORC1 that remodels cancer cell bioenergetics to augment neoplastic
84 growth.

85

86 ***ETFDH* abrogation accelerates tumor growth**

87 ETFDH is essential in skeletal muscle cells [8]. Intriguingly, a CRISPR-Cas9 knock out (KO)
88 screen performed in a human acute lymphoblastic leukemia cell line (NALM6) [9] ranked *ETFDH*
89 as a top non-essential metabolic gene that clustered with well-established tumor suppressors *TP53*
90 and *RB1* (Supplementary Fig.1B). Mining DepMap also revealed that *ETFDH* is essential in only
91 1 out of 1150 cancer cell lines [10]. This motivated us to examine the role of ETFDH in cancer.

92 *ETFDH* mRNA levels are reduced in patient samples across different cancer types, including colon
93 (Supplementary Fig.1C) and breast cancer (Supplementary Fig.1D). Immunohistochemistry (IHC)
94 staining confirmed that ETFDH protein levels are significantly reduced in colorectal cancer vs.
95 non-adjacent patient-derived tissues (NAT) (Fig.1A).

96 We next abrogated the *ETFDH* gene using a CRISPR-Cas9 approach in a variety of cancer
97 cell lines including HCT-116 (human colorectal cancer), NT2197 (murine HER2+ breast cancer),
98 4T1 (murine triple negative breast cancer cells), and NALM6 cells (Supplementary Fig.1E-H). We
99 also investigated the effects of ETFDH loss in non-transformed normal murine mammary gland
100 (NMuMG) cells (Supplementary Fig.1I), a parental immortalized mammary epithelial cell line that
101 was transformed with an oncogenic ErbB2 variant to generate NT2197 cells [11]. Notwithstanding
102 their high baseline proliferation rates, ETFDH ablation significantly increased proliferation across
103 all tested cancer cell lines (Supplementary Fig.1E-H). This was not caused by the inadvertent
104 effects of the CRISPR-Cas9, as rescuing ETFDH expression in HCT-116 and NT2197 cells
105 reverted proliferation rates to levels comparable to ETFDH-proficient controls (Supplementary
106 Fig.1E-F). In contrast, ETFDH abrogation did not affect proliferation of non-transformed
107 NMuMG cells (Supplementary Fig.1I). ETFDH KO HCT-116 cells also formed more colonies in
108 soft agar (surrogate measurement of cellular neoplastic potential [12]) as compared to empty vector
109 infected controls (WT EV), and ETFDH KO cells in which ETFDH was re-expressed (ETFDH
110 Rescue) (Supplementary Fig.1J).

111 Based on these findings, we tested the impact of ETFDH loss on neoplastic growth *in vivo.*
112 WT EV, ETFDH KO, or ETFDH Rescue HCT-116 cells were injected orthotopically in the caeca
113 of SCID-BEIGE mice. Loss of ETFDH significantly increased the tumor growth rate and volume
114 at endpoint relative to control and ETFDH Rescue cells (Fig.1B-C). ETFDH loss also increased

115 NT2197 tumor growth and the final tumor volume as compared to ETFDH-proficient tumors
116 following orthotopic mammary fat pad injections in SCID-BEIGE mice (Fig.1D-E). Altogether,
117 these results show that *ETFDH* is an non-essential gene in cancer that is under-expressed across
118 different cancer types, and that its disruption enhances neoplastic growth, while not affecting
119 proliferation of non-transformed cells.
120

121 **ETFDH abrogation results in ETF insufficiency that paradoxically increases bioenergetic**
122 **capacity of cancer cells**

123 In non-cancerous cells, ETFDH transfers electrons from catabolism of fatty acids and amino acids
124 to the ETC (Supplementary Fig.2A). Palmitate oxidation (monitored by oxygen consumption) and
125 ^{13}C leucine labelling into citrate (citrate m+2) were strongly attenuated by ETFDH abrogation in
126 HCT-116 cells (Supplementary Fig.2B-C), which confirmed that ETF plays a role in fatty and
127 amino acid catabolism in malignant cells. Thus, ETFDH loss induces ETF insufficiency in cancer
128 cells that mirrors defects observed in non-malignant tissues. Surprisingly, ETFDH loss in HCT-
129 116 cells increased oxygen consumption and extracellular acidification, relative to control WT EV
130 and ETFDH Rescues (Fig.2A-B). ETFDH KO HCT-116 cells produced higher levels of ATP from
131 oxidative phosphorylation (*J* ATP ox) as compared to ETFDH-proficient cells (Fig.2C-D).
132 Consequently, ETFDH loss increased the bioenergetic capacity of HCT-116 cells (Fig.2E).
133 Comparable results were observed in NT2197 cells (Supplementary Fig.2D-H). Collectively, these
134 findings suggest that although ETF insufficiency limits the ability of cancer cells to utilize lipids
135 and amino acids, it paradoxically upregulates their mitochondrial metabolism and bioenergetic
136 capacity.

137 Glutamine plays an important role in fueling mitochondrial metabolism and *de novo* nucleotide
138 biosynthesis to support cancer cell proliferation[13]. ETFDH abrogation increased glutamine uptake
139 and glutamate production in both HCT-116 (Fig.2F) and NT2197 (Supplementary Fig.2I) cells.
140 ETFDH loss increased ^{13}C-glutamine incorporation in the forward direction (green) and the
141 reverse direction (purple) of the citric acid cycle (CAC; Fig.2G-H, Supplementary Fig.2J),
142 suggesting higher glutamine tracing into the CAC, as well as increased reductive glutamine
143 metabolism. Indeed, the steady state levels of several nucleotides were also increased following
144 ETFDH loss (Supplementary Fig.2K). To highlight the dependence of glutamine in contributing
145 to the proliferation of cells upon ETFDH abrogation, HCT-116 WT EV and ETFDH KO cells
146 were grown in the absence or presence of glutamine. Accordingly, ETFDH KO HCT-116 cells
147 exhibited greater sensitivity to glutamine deprivation than control WT EV cells (Fig.2I).
148 Collectively, these data demonstrate that ETF insufficiency in cancer cells remodels mitochondrial
149 metabolism and increases the glutamine consumption and anaplerosis.
150

151 **ETFDH loss induces intracellular accumulation of amino acids, mTOR signaling and protein**
152 **synthesis**

153 Consistent with the established role of ETFDH in amino acid catabolism [2], and reduction of leucine
154 consumption upon ETFDH abrogation (Supplementary Fig.2C), steady state levels of most
155 intracellular amino acids were increased in ETFDH KO vs. WT HCT-116 and NT2197 cells
156 (Fig.3A). Moreover, ETFDH-deficient HCT-116 cells exhibited higher rates of protein synthesis
157 relative to ETFDH-proficient cells (Fig.3B). Amino acids activate the mechanistic target of
158 rapamycin (mTOR) which stimulates protein synthesis [14]. Indeed, mTORC1 signaling was higher
159 in ETFDH-deficient than ETFDH-proficient HCT-116 and NT2197 cells as illustrated by

160 increased phosphorylation of ribosomal protein S6 kinases (S6K1/2; Thr389) and their substrate
161 ribosomal protein S6 (rpS6; Ser240/244) (Fig.3C). Re-expression of ETFDH in ETFDH KO cells
162 resulted in normalization of mTORC1 signaling to the levels observed in WT EV cells (Fig 3D).
163 mTORC2 signaling was also augmented upon ETFDH abrogation in HCT-116 and NALM6 cells
164 as evidenced by increased AKT phosphorylation (Ser473) (Supplementary Fig.3A-B). Despite
165 bioenergetic rewiring, ETFDH loss did not exert a major effect on the activity of adenosine
166 monophosphate-activated protein kinase (AMPK) as monitored by its phosphorylation (Thr172)
167 or phosphorylation of its substrate acetyl-CoA carboxylase (ACC at S79) (Supplementary Fig.3A-
168 B).

169 Consistent with mTOR hyperactivation, ETFDH KO HCT-116 cells were more sensitive
170 to the active site mTOR inhibitor Torin1 [15] as compared to their ETFDH-proficient counterparts
171 (Supplementary Fig.3C). To further determine which mTOR complex is responsible for mediating
172 the hyper-proliferative phenotype triggered by ETFDH loss, we selectively inactivated mTORC1
173 or mTORC2 by depleting RAPTOR or RICTOR, respectively using small hairpin RNA (shRNA)
174 in WT and ETFDH KO HCT-116 cells (Supplementary Fig.3D). Depletion of RAPTOR, but not
175 RICTOR strongly attenuated the proliferation of ETFDH KO cells (Supplementary Fig.3E-F).
176 Moreover, the anti-proliferative effects of bisteric mTORC1-specific inhibitor BiS-35x [16] were
177 stronger in ETFDH KO vs. ETFDH Rescue HCT-116 cells (Supplementary Fig.3G). Altogether,
178 these data suggest that mTORC1, but not mTORC2 acts as a major mediator of hyper-proliferative
179 phenotype triggered by ETFDH loss in cancer cells. Accordingly, the effects of amino acid
180 deprivation on phospho-rpS6 (Ser240/244), and phospho-4E-BP1 (Ser65) were attenuated in
181 ETFDH KO vs. WT control cells, which is consistent with the intracellular accumulation of amino
182 acids upon ETFDH disruption (Fig.3E-G). In turn, serum stimulation (Stim) resulted in

183 comparable induction in phosphorylation of rpS6 (Ser240/244) and 4E-BP1 (Ser65) in ETFDH-
184 deficient and proficient cells (Fig.3E). Collectively, these findings suggest that ETFDH loss
185 induces mTORC1 signaling at least in part by increasing intracellular amino acid levels.

186 Amino acid deprivation leads to general control nonderepressible 2 (GCN2)-dependent
187 phosphorylation of the alpha subunit of eIF2 and subsequent induction of activating transcription
188 factor 4 (ATF4) synthesis during the integrated stress response (ISR) [17]. Consistent with an
189 increase in intracellular amino acid, phosho-eIF2α (S51) levels appeared to be modestly reduced
190 in ETFDH-deficient vs. proficient HCT-116 cells under both serum starvation and amino acid
191 depletion (Supplementary Fig.3H). However, the ETFDH status in the cells did not affect ATF4
192 levels at baseline or upon amino acid depletion (Supplementary Fig.3H). Altogether, these data
193 demonstrate that ETFDH loss induces mTORC1 signaling and protein synthesis, which appears to
194 be at least in part driven by intracellular accumulation of amino acids.

195

196 **ETFDH loss diminishes 4E-BP1, but not 4E-BP2 protein levels**

197 mTORC1 positively controls cell proliferation through the eukaryotic translation initiation factor
198 4E-binding proteins (4E-BPs; 4E-BP1-3 in mammals) [18]. Of note, 4E-BP3 is expressed in a tissue-
199 restricted manner, and does not appear to play a major role in regulating proliferation [18]. mTORC1
200 phosphorylates 4E-BPs to promote eukaryotic translation initiation factor 4F (eIF4F) complex
201 assembly by dissociating 4E-BPs from eIF4E, thereby stimulating cap-dependent translation
202 initiation [19]. Consistent with the increased mTORC1 activity, ETFDH-deficient cells exhibited
203 increased phosphorylation of 4E-BP1 (Ser65), which was rescued upon re-expression of ETFDH
204 in HCT-116 and NT2197 cells (Fig.4A). Unexpectedly, we observed that ETFDH loss coincided
205 with a dramatic reduction in total 4E-BP1 protein levels in HCT-116 (Fig.4A), NT2197 (Fig.4A),

206 NALM6 (Supplementary Fig.4A), and 4T1 cells (Supplementary Fig.4B). We also treated WT and
207 ETFDH KO HCT-116 cell lysates with λ-phosphatase to exclude potential confounding effects of
208 different 4E-BP1 phosphorylation states, which confirmed that disruption of ETFDH is paralleled
209 by reduction in 4E-BP1 levels (Fig.4B). Notably, loss of ETFDH did not exert a major effect on
210 4E-BP2 protein abundance in HCT-116 (Fig.4A), NT2197 (Fig.4A), or 4T1 cells (Supplementary
211 Fig.4B). In addition, 4E-BP1, but not 4E-BP2 protein levels were reduced in ETFDH-deficient
212 HCT-116 as compared to WT tumors (Fig.4C-E). Strikingly, loss of ETFDH in non-transformed
213 NMuMG cells did not exert a major effect on mTORC1 signaling (Supplementary Fig.4C) and
214 failed to alter 4E-BP1 protein levels (Supplementary Fig.4C). Collectively, these findings indicate
215 that ETF insufficiency is paralleled by a selective decrease in 4E-BP1 protein levels in cancer, but
216 not non-transformed cells.
217
218 **Decrease in 4E-BP1 protein levels underpins the bioenergetic rewiring induced by ETF**
219 **insufficiency in cancer cells.**
220 Considering that in mammals 4E-BPs play a major role in mediating the effects of mTORC1 on
221 proliferation, neoplastic growth, mitochondrial functions and protein synthesis [18,20,21], we next
222 investigated whether the observed decrease in 4E-BP1 levels contributes to increased proliferation
223 and tumor growth caused by ETFDH abrogation. To this end, we overexpressed 4E-BP1 protein
224 in ETFDH-deficient NT2197 cells by infecting them with a retrovirus wherein *EIF4EBP1*
225 expression was driven by an exogenous promoter [18]. Importantly, 4E-BP1 overexpression in
226 ETFDH KO NT2197 cells decreased eIF4F complex assembly, as evidenced by m^7-GTP pulldown
227 (Fig.4F). 4E-BP1 overexpression also reduced oxygen consumption in ETFDH KO NT2197 cells,
228 relative to empty vector infected cells (Fig.4G). Moreover, restoring 4E-BP1 protein levels

229 decreased cell proliferation (Supplementary Fig.4D) and anchorage-independent growth
230 (Supplementary Fig.4E) of ETFDH KO HCT-116 cells. Lastly, 4E-BP1 overexpression decreased
231 growth and the final volume of tumors formed by NT2197 ETFDH KO cells in SCID-BEIGE mice
232 (Fig.4H-I). Collectively, these data indicate that decreased 4E-BP1 protein levels mediate the pro-
233 neoplastic effects of ETF insufficiency.

234 The mTORC1/4E-BP axis stimulates mitochondrial biogenesis and metabolism by altering
235 the translation of nuclear-encoded mitochondrial mRNAs including mitochondrial transcription
236 factor A (TFAM) [21,22]. ETFDH loss increased mitochondrial DNA levels (Fig.4J) and mass
237 (Supplementary Fig.4F) which was paralleled by TFAM induction (Fig.4K). Collectively, these
238 data show that the loss of 4E-BP1 plays a prominent role in mediating the effects of ETF
239 insufficiency on bioenergetic reprogramming of cancer cells.

240

241 **ETFDH loss decreases *EIF4EBP1* transcription via BCL-6**

242 We next set out to determine the level(s) at which 4E-BP1 protein levels are downregulated in
243 ETF insufficient cancer cells. ETFDH loss did not have a major effect on 4E-BP1 protein synthesis
244 or turnover (Supplementary Fig.4G-H), but it decreased the *EIF4EBP1* mRNA levels in ETFDH-
245 deficient vs. ETFDH-proficient HCT-116 (Fig.4L) and NT2197 cells (Fig.4M). *EIF4EBP1* and
246 *ETFDH* mRNA levels were also positively correlated in tumors isolated from colorectal
247 adenocarcinoma patients (Supplementary Fig.4I). In turn, consistent with no apparent differences
248 in 4E-BP2 protein levels, the levels of *EIF4EBP2* mRNA were unaffected by the ETFDH status
249 in both cell lines (Fig.4L-M). Notably, observed decrease in *EIF4EBP1* mRNA levels was not
250 caused by the effects of ETFDH loss on mRNA stability (Supplementary Fig.4J). Based on these
251 data, we concluded that ETFDH abrogation is paralleled by suppression of *EIF4EBP1*

252 transcription and sought to identify transcription factors that may mediate the effects of ETFDH
253 abrogation on suppression of *EIF4EBP1* expression. ATF4, Snail and Slug have been shown to
254 stimulate transcription of *EIF4EBP1*, but not *EIF4EBP2* [23,24]. However, ATF4, Snail and Slug
255 proteins remain unchanged upon ETFDH disruption (Supplementary Fig.3H, Supplementary
256 Fig.5A). We also re-analyzed publicly available RNA-seq datasets, which revealed that
257 *EIF4EBP1,* but not *EIF4EBP2* expression was increased following STAT1 abrogation in MT4788
258 breast cancer cells [25]. Indeed, we observed that MT4788 STAT1 KO cells have increased 4E-BP1
259 protein levels relative to parental cells (Supplementary Fig.5B). Accordingly, ETFDH KO cells
260 displayed increased STAT1 and downregulated 4E-BP1 protein levels (Supplementary Fig.5C).
261 To determine the impact of STAT1 on *EIF4EBP1* or *EIF4EBP2* promoter occupancy, we
262 performed chromatin immunoprecipitation qPCR (ChIP-qPCR) assay in control (WT EV),
263 ETFDH KO, or ETFDH rescue HCT-116 cells (Supplementary Fig.5D-E). Binding of STAT1 was
264 however comparable to IgG across all tested cell lines thereby suggesting that is unlikely that
265 STAT1 directly suppresses *EIF4EBP1* transcription in the context of ETFDH loss (Supplementary
266 Fig.5D-E). Furthermore, reactive oxygen species (ROS) can also influence redox-responsive
267 transcription [26]. Although loss of ETFDH induced ROS levels (Supplementary Fig.5F), 4E-BP1
268 protein abundance was not altered following treatment with the antioxidant N-acetyl-cysteine
269 (NAC) (Supplementary Data Fig.5G).

270 We next investigated the potential role of B-cell lymphoma 6 (BCL-6) [27-29], which was
271 previously suggested to suppress *EIF4EBP1* transcription [30]. Notably, *ETFDH* abrogation in HCT-
272 116 and NT2197 cells resulted in a marked increase in BCL-6 protein levels, compared to ETFDH-
273 proficient control cells (Fig.5A). These changes in BCL-6 protein levels were mTOR-sensitive
274 (Fig.5B) and not accompanied by the alterations in *BCL6* mRNA abundance (Fig.5C), which is

275 consistent with recently reported mTOR-dependent translational activation of BCL-6 [31-33]. Indeed,
276 *BCL6* mRNA translation was increased in HCT-116 ETFDH KO relative to WT cells (Fig.5D).
277 Taken together, these data point out that ETFDH disruption induces BCL-6 protein synthesis in an
278 mTOR-dependent manner. ETF insufficiency increased BCL-6 binding to the *EIF4EBP1*, but not
279 the *EIF4EBP2* promoter (Fig.5E-F). BCL-6 silencing in NT2197 and 4T1 ETFDH KO cells
280 increased 4E-BP1 protein levels (Fig.5G-H). Depletion of BCL-6 also attenuated proliferation of
281 4T1 ETFDH KO cells (Fig.5I). Collectively, these findings show that BCL-6 mediates the effects
282 of ETF insufficiency on reduction in *EIF4EBP1* expression and increased proliferation of cancer
283 cells.
284
285 **ETFDH acts as a haploinsufficient tumor suppressor.**
286 Data available in cBioPortal from 2683 samples across cancer types [34] indicate that missense or
287 truncating mutations in ETFDH are rare (0.3%) (Fig.6A). This suggests that ETFDH is not lost,
288 but rather downregulated in human cancers. We observed that DNA methylation inhibitors, 5-
289 azacytidine (5-aza) and 5-aza-2′-deoxycytidine (5-aza-2-deoxyC) increased ETFDH protein levels
290 in HCT-116 cells (Fig.6B), thus suggesting that one of the potential mechanisms of downregulated
291 *ETFDH* expression in neoplasia may stem from increased DNA methylation. Based on these
292 observations, we developed a model that more closely reflects ETFDH downregulation, but not a
293 complete loss, in human tumors using a method based on targeted poly(A) track insertion within
294 endogenous genes [35]. The length of the poly(A) track directly correlates with the reduction in
295 amount of protein produced, allowing for the investigation of gene-dosage effects on ensuing
296 phenotypes [35,36]. Accordingly, mutants were designed by inserting poly(A) tracks of 12 and 18
297 adenosines [12A, equivalent to 4 consecutive AAA (Lys) codons $(AAA)_4$; 18A, equivalent to 6

298 consecutive AAA (Lys) codons $(AAA)_6$], as well as a control track (CTRL) [6 consecutive lysine
299 AAG codons $(AAG)_6$] (Supplementary Fig.6A, see methods). Based on an Alphafold rendered
300 structure (version 2) [37,38], we chose residue 38 in an unstructured loop as an insertion site
301 (Supplementary Fig.6B). Of note, $(AAA)_6$ and $(AAG)_6$ stretches are translated in the equal number
302 of Lys residues, whereby (AAA), but not (AAG), stretches decrease ETFDH protein levels
303 (Fig.6C). $(AAG)_6$ construct was thus used as a control to mitigate potential inadvertent effects of
304 the insertion of poly-Lys on the ETFDH function. $(AAA)_4$ and $(AAA)_6$ stretches progressively
305 reduced ETFDH protein abundance as compared to constructs harboring the $(AAG)_6$ track
306 (Fig.6C). The reduction in ETFDH protein levels was mirrored by a gene-dose dependent increase
307 in mTORC1 signaling, BCL-6 expression and reduction in 4E-BP1, but not 4E-BP2 protein levels
308 (Fig.6C). Accordingly, *Eif4ebp1* mRNA levels were reduced in *ETFDH* dose-dependent manner,
309 while *Eif4ebp2* mRNA levels remained unaffected (Fig.6D). Moreover, reduction in ETFDH
310 protein levels correlated with increased mtDNA content (Fig.6E), oxygen consumption (Fig.6F),
311 ATP production from OXPHOS (JATPox) (Fig.6G), bioenergetic capacity (Fig.6H), and cell
312 proliferation (Fig.6I). Finally, ETFDH KO NT2197 tumors carrying $(AAA)_6$ insertions exhibit
313 increased tumor growth and larger final tumor volumes relative to control tumors expressing
314 $(AAG)_6$ insertions in SCID-BEIGE mice (Fig.6J-K). Altogether, these findings show that ETFDH
315 gene-dosage influences neoplastic growth, thus suggesting that ETFDH may act as a
316 haploinsufficient tumor suppressor.
317 Lastly, we determined whether the catalytic activity of ETFDH is required for its tumor
318 suppressive activity. To achieve this, we re-expressed WT or ETFDH mutant (Y304A,G306E)
319 with disrupted catalytic activity [8] in HCT-116 ETFDH KO cells. Notwithstanding that both
320 ETFDH variants were expressed to comparable levels, in contrast to WT, ETFDH (Y304A,G306E)

321 mutant failed to suppress mTORC1 signaling and decrease 4E-BP1 levels (Supplementary Figure
322 6C), reduce proliferation (Supplementary Fig.6D) or perturb the bioenergetic profiles of HCT-116
323 ETFDH KO cells (Supplementary Fig.6E-F). Taken together, these data suggest the catalytic
324 activity of ETFDH is required for its tumor suppressive actions.
325
326 **Discussion**
327 Notwithstanding that ETFDH mutations play a detrimental role in MADD metabolic disorders, we
328 show that ETF insufficiency caused by reduced *ETFDH* expression plays a major role in rewiring
329 cancer metabolism and signaling to stimulate neoplastic growth. Reduction of ETFDH levels
330 appears to be a common feature of cancer cells and is likely a consequence of DNA
331 hypermethylation (Fig.6B), an event that is frequently observed among tumor suppressor genes [39].
332 Indeed, ETFDH was found among the most under-expressed metabolic enzymes in a study that
333 compiled cancer microarray datasets [40]. Moreover, recent studies highlighted crosstalk between
334 aberrant mTOR signaling and epigenetic perturbations [41-44], which further reinforces the
335 plausibility that epigenetic reprograming in cancer cells may underpin the pro-neoplastic role of
336 ETFDH downregulation and/or explain resulting phenotypes.
337 Intriguingly, although ETF insufficiency limits the flexibility of cancer cells in using fuels
338 (e.g., lipids and amino acids) for OXPHOS, it triggers signalling events that establish a feed-
339 forward loop via mTORC1, leading to increased BCL-6 levels and reduced *EIF4EBP1*
340 transcription (Fig.6L). ETF insufficiency thus orchestrates enhanced mTORC1 signaling with
341 downregulation of 4E-BP1 protein levels to reprogram protein synthesis and ultimately increase
342 mitochondrial biogenesis and functions thereby providing a selective proliferative advantage to
343 cancer cells (Fig.6L). To this end, ETF insufficiency allows cancer cells to trade their metabolic

344 flexibility for increased bioenergetic capacity and a re-wired signaling state that favors neoplastic
345 growth. Importantly, while ETFDH plays an essential role in muscle, we did not observe a major
346 effect of ETFDH disruption on proliferation, mTOR signaling or 4E-BP1 levels in non-
347 transformed murine breast epithelial NMuMG cells. These observations suggest that ETF
348 insufficiency causes remodeling of signaling and metabolic networks that are favourable to cancer
349 cells.

350 Our findings are consistent with previously attributed tumor-suppressive effects of 4E-BP1
351 [45-50]. More recently, it has been demonstrated that under certain contexts 4E-BPs may play a
352 beneficial role for tumor survival. For instance, 4E-BPs may facilitate tumor growth by regulating
353 global and selective mRNA translation under periods of cellular stress [51,52], including suppression
354 of fatty acid biosynthesis under glucose deprivation [53,54]. Collectively, these findings demonstrate
355 that 4E-BPs are likely to play more complex, context dependent roles during cancer progression
356 than previously anticipated. Moreover, the role of different 4E-BP proteoforms in cancer was in
357 general thought to be redundant. Our findings however demonstrate that in the context of ETF
358 insufficiency selective decrease in 4E-BP1, but not 4E-BP2 levels plays a role in driving neoplastic
359 growth thereby suggesting that 4E-BP1 and 4E-BP2 may play hitherto unappreciated non-
360 overlapping roles in neoplasia.

361 Several metabolites can be sensed via signaling partners upstream of mTORC1, including
362 leucine, arginine, methionine/SAM, and threonine [55]. Branched-chain amino acids (leucine,
363 isoleucine, and valine), which are among the highest upregulated metabolites in ETFDH deficient
364 cells (Fig 3A) serve as ETFDH substrates, and have been described to display strong activation
365 capabilities towards mTORC1 in the literature [56,57]. Glutamine can also activate mTORC1 through
366 Arf family of GTPases [58]. Indeed, glutamine can supplement the non-essential amino acid (NEAA)

367 pool through transamination [59] and amino acid uptake [60]. Accordingly, the maintenance of NEAA
368 that are non-ETFDH substrates may be supported by the global metabolic rewiring fueled by
369 enhanced glutamine metabolism in ETFDH-deficient cells. Deciphering the mechanisms leading
370 to accumulation of specific amino acids and their role in ETFDH-dependent mTORC1 modulation
371 is warranted.

372 In conclusion, we show that ETF insufficiency caused by reduced ETFDH expression
373 remodels signaling and mitochondrial metabolism in a manner that drives neoplastic growth
374 (Fig.6L), while either being neutral (NMuMG) or deleterious (muscle cells) in non-malignant cells.
375 These findings explain how disruption of mitochondrial enzyme, rather than reducing cellular
376 fitness, is common in cancer because it increases mitochondrial energy flux to drive neoplastic
377 growth.

378 Figure 1: ETFDH loss promotes tumor growth

379 A) ETFDH protein levels in non-adjacent tissue (NAT) or grade 3 cancerous tissue (Tumor) were
380 determined by immunocytochemistry (IHC) of colorectal cancer tissue microarray. Staining
381 intensity of DAB in arbitrary units (A.U) is shown. Data are presented as means +/- SEM (NAT
382 n=14, Tumor n=13), **$p<0.01$, unpaired Student's *t* test.

383 B-C) Tumor growth of WT EV, ETFDH KO, and ETFDH Rescue HCT-116 cells following intra-
384 caecal injection (B) and endpoint tumor volumes (C). Growth was assessed by luminescence
385 (photons). Data are presented as means +/- SEM (WT EV n=6, ETFDH KO n=8, ETFDH Rescue
386 n=8), *$p<0.05$, one-way ANOVA, Tukey's post-hoc test.

387 D-E) Tumor growth of WT and ETFDH KO NT2197 cells following mammary fat-pad injection
388 (D) and endpoint tumor volumes (E). Growth was assessed using a caliper. Data are presented as
389 means +/- SEM (WT n=17, ETFDH KO n=17), *$p<0.05$, unpaired Student's *t* test.

390 Figure 2: Absence of ETFDH promotes mitochondrial metabolism

391 A-B) Oxygen consumption (A) and extracellular acidification (B) in WT EV, ETFDH KO, and
392 ETFDH Rescue HCT-116 cells were determined using a Seahorse bioanalyzer. Data are
393 normalized to cell count and presented as means +/- SD (n=4), *p<0.05, **p<0.01, one-way
394 ANOVA, Tukey's post-hoc test.

395 C) Basal *J* ATP calculations from WT EV, ETFDH KO, and ETFDH Rescue HCT-116 cells. *J*
396 ATP ox represents ATP production from oxidative phosphorylation, while *J* ATP glyc is ATP
397 production from glycolysis. Comparison between *J* ATP ox (grey bars; top) and *J* ATP glyc (white
398 bars; bottom) is shown. Data are presented as means +/- SD (n=4), *p<0.05, **p<0.01, one-way
399 ANOVA, Tukey's post-hoc test.

400 D-E) Bioenergetic plot for Basal, FCCP, and Monensin *J* ATP fluxes (D) and bioenergetic capacity
401 (E) of WT EV, ETFDH KO, and ETFDH Rescue HCT-116 cells. Data are presented as means +/-
402 SD (n=4), *p<0.05, one-way ANOVA, Tukey's post-hoc test.

403 F) Glutamine uptake and glutamate production in WT and ETFDH KO HCT-116 cells. Results
404 are shown as fold changes of ETFDH KO cells relative to WT cells. Data are presented as means
405 +/- SD (n=3), *p<0.05, paired Student's *t* test.

406 G) Schematic of ^{13}C-glutamine tracing throughout the citric acid cycle (CAC). Isotopomers
407 labelled in green depict ^{13}C-glutamine tracing in the forward direction of the CAC, while those in
408 purple represent reverse tracing.

409 H) Relative abundance of ^{13}C-labelled metabolites in the forward (green) and reverse (purple)
410 directions from WT (blue) and ETFDH KO (red) NT2197 cells. Data are presented as means +/-
411 SD (n=3), *p<0.05, **p<0.01, ***p<0.001, ****p<0.0001, paired Student's *t* test.

412 I) Proliferation of WT and ETFDH KO HCT-116 cells grown in the absence or presence of
413 glutamine for 48 hours. Results are shown as fold changes of cell counts under glutamine
414 deprivation relative to those under glutamine repleted conditions. Data are presented as means +/-
415 SD (n=3), *$p<0.05$, paired Student's *t* test.

416 Figure 3: ETFDH loss bolsters mTORC1 signaling and downregulates 4E-BP1 protein levels.

417 A) Amino acid profile in WT and ETFDH KO HCT-116 and NT2197 cells. Data are presented as
418 fold change in amino acid levels in ETFDH KO compared to WT cells (n=3).

419 B) Puromycin incorporation assays in WT and ETFDH KO HCT-116 cells. Levels and
420 phosphorylation status of indicated proteins were determined via western blotting using indicated
421 antibodies. β-Actin was used as a loading control (representative blots of n=3). Quantification of
422 puromycin incorporation is presented as fold change in ETFDH KO vs. WT cells.

423 C) Levels and phosphorylation status of indicated proteins in WT or ETFDH KO HCT-116 and
424 NT2197 cells were determined by western blotting. β-Actin served as a loading control
425 (representative blots of n=3).

426 D) Levels and phosphorylation status of indicated proteins in WT EV, ETFDH KO, or ETFDH
427 Rescue HCT-116 and NT2197 cells were determined by western blotting. β-Actin was used as a
428 loading control (representative blots of n=3).

429 E) Total and phosphoprotein levels in WT or ETFDH KO HCT-116 cells were determined by
430 western blotting using indicated proteins. Cells were serum starved overnight, then depleted of
431 amino acids for indicated timepoints (0, 10, 30, 60 minutes), or stimulated with FBS for 4 hours
432 (Stim). β-Actin was used as loading control (representative blots of n=3).

433 F) Quantification of pS6(S240/244)/S6 ratio from data presented in panel E. Data are presented as
434 means +/- SD (n=3), *$p<0.05$, one-way ANOVA, Tukey's post-hoc test.

435 G) Quantification of p4E-BP1(S65)/4E-BP1 ratio from data presented in panel E. Data are
436 presented as means +/- SD (n=3), *$p<0.05$, one-way ANOVA, Tukey's post-hoc test.

437 Figure 4: Repression of *EIF4EBP1* transcription mediates the effects of ETFDH loss on cancer
438 bioenergetics and tumor growth
439 A) Levels and phosphorylation status of indicated proteins in WT EV, ETFDH KO, or ETFDH
440 Rescue HCT-116 and NT2197 cells were determined by western blotting. β-Actin was used as a
441 loading control (representative blots of n=3).
442 B) Levels of indicated protein in λ-phosphatase treated WT or ETFDH KO HCT-116 and NT2197
443 cell lysates were monitored by western blotting. β-Actin was used as a loading control
444 (representative blots of n=3).
445 C) Indicated protein levels in WT or ETFDH KO HCT-116 tumors were determined by western
446 blotting. AKT was used as loading control (WT n=8, ETFDH KO n=11).
447 D-E) Quantification of 4E-BP1 (D) and 4E-BP2 (E) from tumors described in panel C. Data are
448 presented as means +/- SEM (WT n=8, ETFDH KO n=11), ***$p<0.001$, unpaired Student's *t* test.
449 F) m^7GDP pulldown assay in ETFDH KO and ETFDH KO overexpressing 4E-BP1 (ETFDH KO
450 4E-BP1) NT2197 cells. Specified protein levels in m^7GDP pulldown or input were determined by
451 western blot. β-Actin was used as loading control (input) and to exclude contamination in the
452 pulldown material (m^7GTP bound) (representative blots of n=3).
453 G) Oxygen consumption of ETFDH KO and ETFDH KO 4E-BP1 NT2197 cells. Data are
454 normalized to cell count and presented as means +/- SD (n=5), **$p<0.01$, Student's *t* test.
455 H-I) Tumor growth of ETFDH KO and ETFDH KO 4E-BP1 NT2197 cells following mammary
456 fat-pad injection (H) and endpoint tumor volumes (I). Growth was assessed using caliper
457 measurements. ETFDH KO measurements are the same as in Fig.1D, as these growth curves were
458 obtained in the same experiment. Data are presented as means +/- SEM (ETFDH KO n=17,
459 ETFDH KO 4E-BP1 n=18), **$p<0.01$, unpaired Student's *t* test.

460 J) Mitochondrial DNA in WT EV, ETFDH KO, and ETFDH Rescue HCT-116 cells was quantified
461 by qPCR. Mitochondrial DNA (mtDNA) content was normalized to genomic DNA (gDNA). Data
462 are presented as fold change relative to WT EV cells +/- SD (n=3), *p<0.05, **p<0.01, one-way
463 ANOVA, Tukey's post-hoc test.
464 K) Levels of indicated proteins in WT EV, ETFDH KO, and ETFDH Rescue HCT-116 cells were
465 assessed by western blotting. β-Actin was used as a loading control (representative blots of n=3).
466 L) *EIF4EBP1* and *EIF4EBP2* mRNA levels in WT EV, ETFDH KO, and ETFDH Rescue HCT-
467 116 cells were determined by RT-qPCR. *PP1A* was used as a house-keeping gene. Data are
468 presented as fold change of *EIF4EBP1/PP1A* and *EIF4EBP2/PP1A* ratios relative to WT EV cells
469 (set to 1) +/- SD (n=3), *p<0.05, one-way ANOVA, Tukey's post-hoc test.
470 M) *Eif4ebp1* and *Eif4ebp2* mRNA abundance in WT and ETFDH NT2197 KO cells was
471 determined by RT-qPCR. *Actb* was used as a house-keeping gene. Data are presented as fold
472 change in *Eif4ebp1/Actb* and and *Eif4ebp2/Actb* ratios relative to WT cells +/- SD (n=3), *p<0.05,
473 paired Student's *t* test.

474 Figure 5: Loss of ETFDH increases BCL-6 levels leading to BCL-6-dependent inhibition of
475 *EIF4EBP1* transcription.
476 A) Levels of indicated proteins in WT or ETFDH KO HCT-116 and NT2197 cells were determined
477 by western blotting. β-Actin was used as a loading control (representative blots of n=3).
478 B) Levels of indicated proteins in ETFDH KO NT2197 cells treated with DMSO or Torin1
479 (250nM) for 4 hours were determined by western blotting. β-Actin was used as a loading control
480 (representative blots of n=3).
481 C) *BCL6/Bcl6* mRNA abundance in WT and ETFDH KO HCT-116 and NT2197 cells was
482 determined by RT-qPCR. *PP1A* mRNA was used as a control for HCT-116 experiments, while
483 *Actb* mRNA was used as a control for NT2197 experiments. Data are presented as fold change in
484 *EIF4EBP1/PP1A* and *EIF4EBP2/PP1A* (HCT-116) and *Eif4ebp1/Actb* and and *Eif4ebp2/Actb*
485 (NT2197) ratios relative to WT cells +/- SD (n=3), paired Student's *t* test.
486 D) Polysome profiling of WT and ETFDH HCT-116 KO cells. The absorbance at 254nm (AU
487 254nm) was used to monitor distribution of the 40S-, 60S- ribosomal subunits, monosomes (80S)
488 and polysomes across the gradient. *BCL6* mRNA abundance from polysome gradient fractions was
489 obtained using RT-qPCR. Data are shown as a mean percentage of mRNA in each fraction relative
490 to cumulative corresponding mRNA amount across the whole gradient +/-SD (n=3).
491 E-F) Binding events of BCL-6 to the promoters of *EIF4EBP1* and *EIF4EBP2* were determined by
492 ChIP-qPCR. IgG was used a negative control. Data are presented as % of input (n=3), *$p<0.05$,
493 two-way ANOVA, Dunnett's post-hoc test.
494 G) The levels of indicated proteins in ETFDH KO NT2197 cells transfected with siRNA targeting
495 BCL-6 (siBCL-6) or control, scrambled siRNA (siCTRL) were determined by western blotting. β-
496 Actin was used as loading control (representative blots of n=2).

497 H) Levels of indicated proteins in ETFDH KO 4T1 cells infected with shRNAs targeting BCL-6
498 (shBCL-6 #1 or shBCL-6#2) or control, scrambled shRNA (shCTRL) were monitored by western
499 blotting. β-Actin served as loading control (representative blots of n=3).
500 I) Proliferation of ETFDH KO shCTRL, shBCL-6 #1, or shBCL-6#2 4T1 cells. Data are presented
501 as cell count means (n=3), *$p<0.05$, one-way ANOVA, Dunnett's post-hoc test.

502 Figure 6: Reduced expression of ETFDH increases mitochondrial metabolism and tumor growth

503 A) ETFDH mutations from 2683 samples across multiple cancer types. Number of missense and
504 truncating mutations are shown relative to samples with no mutations. Data are acquired from the
505 ICGC/TCGA Pan-Cancer Analysis of Whole Genomes Consortium [34], accessed from the
506 cBioPortal server (www.cbioportal.org).

507 B) Levels of indicated proteins in WT HCT-116 cells treated with 2.5μM 5-azacytidine (5-aza),
508 10μM 5-aza-2' -deoxycytidine (5-aza-2-deoxyC), or a vehicle (DMSO) for 72 hours were
509 determined by western blotting. β-Actin was used as a loading control (representative blots of
510 n=3).

511 C) Levels and the phosphorylation status of indicated proteins in ETFDH KO NT2197 cells
512 expressing ETFDH harboring $(AAG)_6$, $(AAA)_4$, $(AAA)_6$ tracks were determined by western
513 blotting. β-Actin was used as a loading control (representative blots of n=3).

514 D) *Eif4ebp1* and *Eif4ebp2* mRNA abundance in $(AAG)_6$, $(AAA)_4$, and $(AAA)_6$ NT2197 cells were
515 determined by RT-qPCR. *Actb* was used as a house-keeping gene. Data are presented as fold
516 change in *Eif4ebp1/Actb* and *Eif4ebp2/Actb* ratios relative to $(AAG)_6$ NT2197 cells (n=3),
517 *p<0.05, **p<0.01, one-way ANOVA, Dunnett's post-hoc test.

518 E) Mitochondrial DNA content in $(AAG)_6$, $(AAA)_4$, and $(AAA)_6$ NT2197 cells were monitored
519 by qPCR. Mitochondrial DNA (mtDNA) content was normalized to genomic DNA (gDNA)
520 content. Data are presented as mean fold change relative to $(AAG)_6$ NT2197 cells -/+ SD (n=3),
521 *p<0.05, **p<0.01, one-way ANOVA, Dunnett's post-hoc test.

522 F) Oxygen consumption of $(AAG)_6$, $(AAA)_4$, and $(AAA)_6$ NT2197 cells was determined using
523 Seahorse bioanalyzer. Data are normalized to cell count and presented as means +/- SD (n=4), one-
524 way ANOVA, Dunnett's post-hoc test.

525 G-H) Bioenergetic Plot for Basal, FCCP, and Monensin *J* ATP fluxes (G) and Bioenergetic
526 Capacity (H) derived from $(AAG)_6$, $(AAA)_4$, and $(AAA)_6$ NT2197 cells. Data are presented as
527 means +/- SD (n=4), one-way ANOVA, Dunnett's post-hoc test.
528 I) Proliferation of $(AAG)_6$, $(AAA)_4$, and $(AAA)_6$ NT2197 cells. ETFDH rescue measurements are
529 the same as in Supplementary Fig.1F. Data are presented as cell count means +/- SD (n=4),
530 **p<0.01, one-way ANOVA, Dunnett's post-hoc test.
531 J-K) Tumor growth of $(AAG)_6$ and $(AAA)_6$ NT2197 cells following mammary fat-pad injection
532 (J) and endpoint tumor volumes (K). Growth was assessed using calipers. Data are presented as
533 means +/- SEM ($(AAG)_6$ n=6-12, $(AAA)_6$ n=11-13), **p<0.01, unpaired Student's *t* test.
534 L) Schematic representation of the model whereby reduction in ETFDH levels accelerates tumor
535 growth. Reduction of ETFDH triggers accumulation of intracellular amino acids thus increasing
536 mTORC1 signaling. This is orchestrated with BCL-6-dependent reduction in 4E-BP1 levels to
537 drive mitochondrial biogenesis and increase bioenergetic capacity of cancer cells ultimately
538 leading to more aggressive tumor growth.

539 Supplementary Figure 1: *ETFDH* expression is reduced across a broad array of cancer subtypes,
540 whereby *ETFDH* is a non-essential gene in cancer cells.
541 A) Schematic of electron transfer from fatty and amino acids towards the electron transport chain
542 (ETC) via electron transfer flavoprotein (ETF) and electron transport flavoprotein dehydrogenase
543 (ETFDH).
544 B) Gene essentiality in NALM6 cells. 19084 genes are presented and ranked based on essentiality
545 (1 being most essential and 19084 being the least essential). Orange bar depicts essential genes
546 and grey bar depicts non-essential genes. The rank of *ETFDH* is compared to those of *MYC*, *NRAS*,
547 *RB1*, and *TP53*.
548 C) *ETFDH* mRNA abundance profiles across tumor samples (red) compared to normal tissues
549 (blue). Data are presented as log2CPM (counts per million). Data were derived from The Cancer
550 Genome Atlas (TCGA) repository and accessed on the GEPIA2 server (http://gepia2.cancer-
551 pku.cn) (Colon Adenocarcinoma: Normal n=349, Tumor n=275; Liver Hepatocellular Carcinoma:
552 Normal n=160, Tumor n=369; Rectal Adenocarcinoma: Normal n=318, Tumor n=92; Ovarian
553 Serous Cystadenocarcinoma: Normal n=88, Tumor n=426; Skin Cutaneous Melanoma: Normal
554 n=558, Tumor n=461; Testicular Germ Cell Tumors: Normal n=165, Tumor n=137; Uterine
555 Carcinoma: Normal n=78, Tumor n=57), $p<2.2x10^{-16}$.
556 D) *ETFDH* mRNA levels across healthy (labelled as normal) and breast tumor (labelled as tumor)
557 samples. RNAseq data from both TCGA and GTex databases were processed and normalized as
558 described. TPM values were downloaded from GEO [GSE86354 (healthy) and [GSM1536837
559 (tumour)]. Expression is presented as log_2 standardised mRNA levels. Data were acquired from
560 the 'Breast cancer gene-expression miner' (bc-GenExMiner) server

561 (http://bcgenex.ico.unicancer.fr) using *ETFDH* expression according to nature of the tissue.
562 (Normal n=92, Tumor n=743). p<0.0001, Dunnett-Tukey-Kramer's test.
563 E-F) Proliferation of WT EV, ETFDH KO, and ETFDH Rescue HCT-116 (E) and NT2197 (F)
564 cells. ETFDH rescue measurements are the same as in Fig.6I. Data are presented as cell count
565 means +/- SD over multiple time-points. Representative western blot of indicated proteins is
566 provided in the inlets (n=3), *p<0.05, **p<0.01, one-way ANOVA, Tukey's post hoc test.
567 G-H) Proliferation of WT and ETFDH KO 4T1 (G) and NALM6 (H) cells. Data are presented as
568 cell count means +/- SD over indicated time-points. Representative western blot of indicated
569 proteins is provided in the inlets (n=3), *p<0.05, paired Student's *t* test.
570 I) Proliferation of WT and ETFDH KO NMuMG cells. Representative western blot of indicated
571 proteins is provided in the inlets (n=3), one-way ANOVA, Dunnett's post hoc test.
572 J) Soft agar/colony formation assays in WT EV, ETFDH KO, and ETFDH Rescue HCT-116 cells.
573 Data are presented as fold change relative to WT EV cells (n=3), *p<0.05, **p<0.01, one-way
574 ANOVA, Tukey's post-hoc test.
575
576
577
578
579
580
581
582
583

584 Supplementary Figure 2: ETFDH loss reprograms mitochondrial bioenergetics

585 A) Schematic depicting fatty acid and leucine catabolism linked to ETFDH electron transfer.

586 B) Palmitate oxidation at basal level in WT EV, ETFDH KO, and ETFDH Rescue HCT-116 cells.

587 Data are presented as means +/- SD (n=6), ****p<0.0001, one-way ANOVA, Tukey's post-hoc

588 test.

589 C) Fractional enrichment (%) of citrate m+2 in WT EV, ETFDH KO, and ETFDH Rescue HCT-

590 116 cells. Data are presented as means +/- SD (n=6), ****p<0.0001, one-way ANOVA, Tukey's

591 post-hoc test.

592 D-E) Oxygen consumption (D) and extracellular acidification (E) for WT and ETFDH KO

593 NT2197 cells was determined using a Seahorse bioanalyzer. Data are normalized to cell count and

594 presented as means +/- SD (n=5), *p<0.05, **p<0.01, paired Student's *t* test

595 F) Basal *J* ATP calculations from WT and ETFDH KO NT2197 cells. *J* ATP ox represents ATP

596 production from oxidative phosphorylation, while *J* ATP glyc is ATP production from glycolysis.

597 Comparison between *J* ATP ox (grey bars; top) and *J* ATP glyc (white bars; bottom) is shown.

598 Data are presented as means +/- SD (n=5), ***p<0.001, paired Student's *t* test.

599 G-H) Bioenergetic Plot for Basal, FCCP, and Monensin *J* ATP fluxes (G) and Bioenergetic

600 Capacity (H) for WT and ETFDH KO NT2197 cells. Data are presented as means +/- SD (n=5),

601 *p<0.05, paired Student's *t* test.

602 I) Glutamine uptake and glutamate production in WT and ETFDH KO NT2197 cells. Data are

603 presented as mean fold changes of ETFDH KO cells relative to WT cells +/- SD (n=3), *p<0.05,

604 paired Student's *t* test.

605 J) Fractional abundance of ^{13}C-labelled metabolites over indicated timepoints from WT (blue) and

606 ETFDH KO (red) NT2197 cells. Isotopomers labelled in green depict ^{13}C-glutamine tracing in the

607 forward direction of the CAC, while those in purple represent reverse tracing. Data are presented
608 as means +/- SD (n=3), *p<0.05, **p<0.01, ***p<0.001, ****p<0.0001, two-way ANOVA,
609 Tukey's post hoc test.
610 K) Nucleotide metabolite profile in WT and ETFDH KO HCT-116 cells monitored by LC-
611 MS/MS. Data are presented as fold change in ETFDH KO compared to WT cells (n=3).
612
613
614
615
616
617
618
619
620
621
622
623
624
625
626
627
628
629

630 Supplementary Figure 3: ETFDH loss increases mTORC1 signaling and dependency

631 A-B) Levels and phosphorylation status of indicated proteins in WT and ETFDH KO HCT-116
632 (A) and NALM6 (B) cells were determined by western blotting. β-Actin was used as a loading
633 control (representative blots of n=3).

634 C) Proliferation of HCT116 ETFDH KO and ETFDH Rescue cells treated with indicated
635 concentrations of Torin1 for 72h. Data are presented as fold changes relative to vehicle (DMSO)
636 treatment (n=3), *p<0.05, **p<0.01, ***p<0.01, two-way ANOVA, Tukey's post hoc test.

637 D) Indicated protein levels in WT and ETFDH KO HCT-116 cells transfected with shRNA
638 targeting *RAPTOR* (shRAPTOR), *RICTOR* (shRICTOR), or scrambled control (SCR) were
639 determined by western blotting. β-Actin was used as a loading control (representative blots of
640 n=3).

641 E-F) Proliferation of HCT-116 WT and ETFDH KO cells expressing SCR and shRAPTOR (E) or
642 SCR and shRICTOR (F). Data are presented as cell count means +/- SD (n=4), **p<0.01,
643 ***p<0.01 two-way ANOVA, Tukey's post hoc test.

644 G) Proliferation of HCT116 ETFDH KO and ETFDH Rescue cells treated with indicated
645 concentrations of BiS-35x for 72 hours. Data are presented as fold changes relative to vehicle
646 (DMSO) treatment (n=3), *p<0.05, **p<0.01, ***p<0.01, two-way ANOVA, Tukey's post hoc
647 test.

648 H) Total and phosphoprotein levels in WT or ETFDH KO HCT-116 cells were determined by
649 western blotting using indicated proteins. Cells were serum starved overnight, then depleted of
650 amino acids for indicated timepoints (0, 10, 30, 60 minutes), or stimulated with FBS for 4 hours
651 (Stim). β-Actin was used as loading control (representative blots of n=3).

652

653 Supplementary Figure 4: *ETFDH* loss induces *EIF4EBP1* transcription

654 A) Protein levels in WT and ETFDH KO NALM6 cells were monitored by western blotting using
655 indicated antibodies. β-Actin was used as a loading control (representative blots of n=3).

656 B) Indicated protein levels in WT and ETFDH KO 4T1 cells were determined by western blotting
657 using indicated antibodies. β-Actin was used as a loading control (representative blots of n=3).

658 C) Protein levels in WT and ETFDH KO NMuMG cells were monitored by western blotting using
659 indicated antibodies. β-Actin was used as a loading control (representative blots of n=3).

660 D) Proliferation of ETFDH KO and ETFDH KO overexpressing 4E-BP1 (ETFDH KO 4E-BP1)
661 HCT-116 cells. Data are presented as cell count means +/- SD over indicated time-points (n=3),
662 **$p<0.01$, paired Student's *t* test.

663 E) Soft agar/colony formation assay in ETFDH KO and ETFDH KO 4E-BP1 HCT-116 cells. Data
664 are presented as fold change relative to ETFDH KO cells (n=3), *$p<0.05$, paired Student's *t* test.

665 F) Mitochondrial mass in WT and ETFDH KO NT2197 cells was monitored by flow cytometry.
666 Data are presented as fold change relative to WT cells (n=3), **$p<0.01$, paired Student's *t* test.

667 G) The levels of indicated proteins in WT and ETFDH KO HCT-116 cells treated with
668 cycloheximide (CHX) (50μg/ml), MG-132 (10μM), or combination thereoff for 4 hours total were
669 monitored by western blotting. β-Actin was used as loading control, whereas p21 was used as a
670 short-lived protein to control for the effects of the CHX and MG-132 treatments (representative
671 blots of n=2).

672 H) Polysome profiling of WT and ETFDH HCT-116 KO cells. Absorbance at 254nm (AU 254nm)
673 was used to monitor the distribution of 40S-, 60S- ribosomal subunits, monosomes (80S) and
674 polysomes across the gradient. Indicated mRNA abundances from polysome gradient fractions

675 was obtained using RT-qPCR. Data are shown as a mean percentage of mRNA in each fraction
676 relative to cumulative corresponding mRNA amount across the whole gradient +/-SD (n=3).
677 I) Correlation between *ETFDH* and *EIF4EBP1* mRNA expression in colon adenocarcinoma
678 samples. Data were derived from TCGA repository.
679 J) WT and ETFDH KO HCT-116 cells were treated with Actinomycin D (10µg/ml) for indicated
680 timepoints upon which *EIF4EBP1* and *GAPDH* mRNA levels were determined by RT-qPCR. Data
681 are presented as a mean percentage of mRNA relative to DMSO-treated cells +/-SD (n=3).
682
683
684
685
686
687
688
689
690
691
692
693
694
695
696

697 Supplementary Figure 5: The effects of ETFDH loss on *EIF4EBP1* transcription are mediated by
698 BCL-6 but not STAT1, Snail or Slug
699 A) Protein levels in WT and ETFDH KO HCT-116 cells were determined by western blotting
700 using indicated antibodies. β-Actin was used as a loading control (representative blots of n=2).
701 B) MT4788 WT and STAT1 KO cells were treated with IFNγ (1ng/ml) to induce STAT1 or vehicle
702 (water) for 24 hours. Levels and phosphorylation status of indicated proteins were determined by
703 western blotting. β-Actin was used as a loading control (representative blots of n=2).
704 C) Protein levels in WT and ETFDH KO HCT-116 cells were assessed by western blotting using
705 annotated antibodies. β-Actin served as a loading control (representative blots of n=3).
706 D-E) Binding of STAT1 to the promoters of *EIF4EBP1* (D) and *EIF4EBP2* (E) was determined
707 by ChIP-qPCR. IgG was used a negative control. Data are presented as a percentage of the input
708 +/- SD (n=3), one-way ANOVA, Tukey's post-hoc test.
709 F) Fluorescence intensity of WT and ETFDH KO HCT-116 cells stained with DCFDA (2μM) and
710 measured by flow cytometry. Median values are depicted in the inlets.
711 G) Levels of 4E-BP1 in WT and ETFDH KO HCT-116 cells were determined by western blotting
712 using the indicated antibody. β-Actin was used as a loading control (representative blots of n=3).
713
714
715
716
717
718
719

720 Supplementary Figure 6: Poly(A) Track design (A-B); ETFDH catalytic activity is required for its
721 tumor suppressive function (C-F)
722 A) Insertion of poly(A) tracks within the coding sequence of murine ETFDH. DNA sequences for
723 constructs $(AAG)_6$, $(AAA)_4$, $(AAA)_6$, and WT Etfdh are shown.
724 B) Protein structure of $(AAG)_6$ / $(AAA)_6$ constructs generated using AlphaFold.
725 C) Levels of indicated proteins in ETFDH KO EV, WT ETFDH rescue (ETFDH WT), and ETFDH
726 mutant Y304A, G306E HCT-116 cells were determined by western blotting. β-Actin was used as
727 a loading control (representative blots of n=2).
728 D) Proliferation of ETFDH KO EV, ETFDH WT, and ETFDH mutant Y304A, G306E HCT-116
729 cells. Data are presented as cell count means +/- SD over indicated time-points (n=3), *$p<0.05$,
730 one-way ANOVA, Tukey's post-hoc test.
731 E-F) Oxygen consumption (E) and extracellular acidification (F) for ETFDH KO EV, ETFDH
732 WT, and ETFDH mutant Y304A, G306E HCT-116 cells was determined using a Seahorse
733 bioanalyzer. Data are normalized to cell count and presented as means +/- SD (n=4), *$p<0.05$, one-
734 way ANOVA, Tukey's post-hoc test.
735
736
737
738
739
740
741
742

743 **Methods**

744 **Cell lines and cell culture**

745 HCT-116, NALM6, and HEK293T cells were obtained from American Type Culture Collection
746 (ATCC) and verified using ATCC Cell line authentication service. NMuMG, NT2197, and
747 MT4788 Parental and STAT1 KO cells were obtained by Dr. J. Ursini-Siegel's lab, while 4T1
748 (4T1-526) cells were obtained from Dr. P.M. Siegel's group. HEK293T and HCT-116 cells were
749 cultured in DMEM supplemented with 10% fetal bovine serum (FBS), 1% penicillin/streptomycin
750 and supplemented with 2mM L-Glutamine to obtain a final concentration of 6mM L-Glutamine.
751 NALM6 and 4T1 cells were cultured in RPMI-1640 supplemented with 10% FBS, 1%
752 penicillin/streptomycin and 2mM L-Glutamine. NMuMG and NT2197 cells were cultured in
753 DMEM supplemented with 10% FBS, 1% penicillin/streptomycin, 2mM L-Glutamine, 10 mg/mL
754 insulin, 20 mM HEPES, pH 7.5. NT2197 culture media was supplemented with puromycin (2
755 µg/mL) as previously described [11]. MT4788 were grown in DMEM, 2.5% FBS, mammary
756 epithelial growth supplement (MEGS), 1% penicillin/streptomycin and gentamycin as previously
757 described [25]. All cell lines were maintained at 37°C and 5% CO2 in a humidified environment and
758 tested periodically for mycoplasma according to the manufacturer's instructions.

759

760 **Animals**

761 6–8-week-old SCID-BEIGE mice were purchased from Charles River. Male SCID-BEIGE mice
762 were used for intracaecal experiments, while female mice were used for mammary fat pad
763 injections. All animal experiments were performed in accordance with the guidelines of the McGill
764 University Animal Ethics Committee and the Canadian Council on Animal Care as approved by
765 the facility animal care committee.

766 **Xenograft Experiments**

767 Luciferase-expressing HCT-116 cells (250,000 cells) were injected intracaecally in male (8-10
768 weeks old) SCID-BEIGE mice as previously described [61]. Tumor growth was monitored and
769 assessed by luminescence (IVIS spectrum, PerkinElmer). Animals were sacrificed after 50 days.
770 Quantification of signal intensity was performed with Living Image software (PerkinElmer).
771 NT2197 mammary tumor cells (50,000 cells) were injected in mammary fat pads of 6-8-week
772 female SCID-BEIGE mice. Tumor growth was monitored using calipers. Measurements were
773 shown as once tumor volume reached 100~200 mm^3 and animals were sacrificed before tumors
774 reached 1cm^3. Tumors were excised, placed in 10% formalin, and embedded for
775 immunohistochemistry.

776

777 **Cell Proliferation Assay**

778 Cells were counted using a Countess automated cell counter (Invitrogen) and trypan blue exclusion
779 was used for determining cell viability. Cells (HCT-116, NT2197, NMuMG, 4T1, NALM-6) were
780 seeded in 6-well dishes and counted to 3-5 days. HCT-116 cells were seeded on day 0 at a density
781 of 100,000 cells for Supplementary Figs.1E, 3C, 3E-G, 4D and 50,000 cells for Supplementary
782 Fig.6D. NT2197 cells were seeded on day 0 at a density of 60,000 cells in Fig.6I and
783 Supplementary Fig.1F. NMuMG cells were seeded on day 0 at a density of 60,000 cells in
784 Supplementary Fig.1I. 4T1 cells were seeded on day 0 at a density of 60,000 cells in Fig.5I and
785 Supplementary Fig.1G. NALM-6 cells were seeded on day 0 at a density of 20,000 cells in
786 Supplementary Fig.1H. For glutamine deprivation experiments, HCT-116 cells were seeded in full
787 culture for 24 hours. The next day, cells were grown in media in the presence or absence of
788 glutamine for 48 hours and then counted. For Torin1/BiS-35x treatment experiments, HCT-116

789 cells were seeded overnight. The next day, media was replaced with treatment media containing
790 Torin1 (50nM, 100nM, 250nM, 500nM) or BiS-35X (1nM, 10nM, 100nM, 1000nM) or DMSO
791 for 72 hours and then counted.
792
793 **Immunohistochemistry**
794 Immunohistochemical staining of colon human parafilm-embedded tissue array
795 (TissueArray.com, CO992b) was performed as previously described [62]. Briefly, the tissue slide
796 was baked for 55°C for 30 min followed by incubation in xylene (2× 5 min), 100% ethanol (2×
797 5 min), 95% ethanol (2× 5 min), 75% ethanol (1× 5min), and ddH_2O (2x 5min). The slide was
798 submerged in 10mM sodium citrate buffer (pH 6.0), 0.05% Tween-20 and heat-induced epitope
799 retrieval was carried out in a pressure cooker for 30 min. The slide was cooled for 20 min at room
800 temperature, rinsed in ddH_2O for 5 min, and washed with 1xTBS + 0.3% Triton X-100 for 10 min,
801 then 1xTBS for 5 min at room temperature. The slide was incubated in 3% H_2O_2 for 10 min at
802 room temperature and washed with TBST (1xTBS + 0.1% Tween-20) for 5 min to inactivate
803 peroxidases. A liquid blocker pen (PAP Pen, DAKO) was used to circle tissues on the slide. The
804 TMA was blocked for 1 hour in room temperature in the presence of DAKO Protein Block-Serum
805 Free (DAKO, Cat#X0909). The slide was incubated overnight at 4°C with the ETFDH antibody
806 (1:500, ProteinTech 11109-1-AP). The next day, the slide was washed in TBST (3x 5min), and
807 secondary incubation was performed for 30 min at room temperature with secondary antibody
808 (Antibody background reducing diluent and HRP rabbit substrate (Cell Signaling, Cat#7074)). The
809 slide was washed in TBST (3x 5min) and DAB (Di-amine-benzidine) peroxidase substrate
810 (Vector, Cat# SK-4100) was applied to the slide for 5 min. Reaction was stopped by washing in
811 ddH_2O for 5 min. The slide was counterstained with filtered hematoxylin for 20 sec and rinsed

812 with ddH_2O for 5 min. The slide was placed in 75% ethanol (1 min), 95% ethanol (1 min), 100%
813 ethanol (1 min) and xylene (2x 5min). The slide was mounted with a cytoseal at 60°C and dried in
814 a fumehood overnight. Quantitation of sections was performed using Imagescope software
815 (Aperio).
816
817 **Western Blotting**
818 Western blotting was performed as previously described [44]. Briefly, cells were washed twice with
819 PBS and lysed with RIPA buffer (50 mM Tris-HCl pH 7.5, 150 mM NaCl, 0.5% sodium
820 deoxycholate, 1 mM PMSF, 1 mM DTT, 1% NP40, 0.1% SDS), supplemented with 1X protease
821 inhibitor (Roche) and 1x PhoSTOP (Roche). Lysates were cleared at 4°C (10min, 13,000rpm).
822 Protein concentrations were determined using BCA kit (ThermoFisher). Lysates were mixed with
823 5x Laemmli buffer (60mM Tris-HCl (pH 6.8), 10% glycerol, 2% SDS, 5% 2-mercaptoethanol,
824 0.05% bromophenol blue) and boiled (95°C for 5min). Proteins were resolved by SDS-PAGE
825 (Bio-Rad) and transferred via wet transfer apparatus (Bio-Rad) to nitrocellulose membranes
826 (Amersham). Membranes were blocked in 5% BSA (dissolved in TBST (0.1% Tween 20 in 1×
827 TBS)) and incubated in primary antibodies overnight at 4°C. The next day, membranes were
828 washed in TBST and incubated with HRP-conjugated secondary antibodies for 1 hour. Membranes
829 were washed and applied with ECL (Bio-Rad) for 1min. Exposure was carried out on an Azure
830 c300 (Azure Biosystems). Images were quantified by ImageJ and analysed using GraphPad
831 Prism10. The list of primary antibodies is described in Supplementary Table 1.
832 For λ-phosphatase experiments, cells were lysed with RIPA and supplemented with 1X
833 protease inhibitor, without 1x PhoSTOP. Protein samples were combined with NEBuffer for

834 protein metallophosphatases (PMP), $MnCl_2$, and λ-protein phosphatase for 30min at 30°C
835 according to the manufacturer's instructions (New England Biolabs).
836
837 **Cap-Binding Pull-Down Assay**
838 Assay was carried out as previously described [18]. Briefly, NT2197 cells were seeded overnight in
839 150mm plates. The next day, media was changed, and cells were washed with PBS and dissolved
840 in lysis buffer containing 50mM MOPS/KOH (7.4), 100mM NaCl, 50 mM NaF, 2mM EDTA,
841 2mM EGTA, 1% NP40, 1% sodium deoxycholate, 7 mM β-mercaptoethanol, supplemented with
842 1X protease inhibitor (Roche) and 1x PhoSTOP (Roche). Lysates were cleared at 4°C (10min,
843 16,000g). Protein concentrations in samples were elucidated by BCA (ThermoFisher). Samples
844 were equilibrated for 20 min rotating at 4°C with m^7-GDP-agarose beads (Jena Bioscience), then
845 washed in buffer containing 50mM MOPS/KOH (7.4), 100mM NaCl, 50 mM NaF, 0.5mM EDTA,
846 0.5 mM EGTA, 7 mM β-mercaptoethanol, 0.5 mM PMSF, 1mM Na_3VO_4 and 0.1mM GTP, by
847 centrifugation (500g for 1min). Bound proteins were eluted from beads via boiling in loading
848 buffer. Western blotting was performed on eluted proteins and input samples to assess for eIF4F
849 complex formation using 4E-BP1, eIF4G1, eIF4E, and β-actin antibodies.
850
851 **Flow Cytometry**
852 NT2197 cells were seeded in 6-well dishes for 24 hours. The next day, cells were stained with
853 50nM MitoTracker Deep Red (ThermoFisher) for 15 minutes at 37°C in the dark. Cells were
854 washed, counted, and 100,000 cells were dissolved in 500µl HBSS (Gibco). Samples were
855 analyzed with the LSR Fortessa cytometer (Becton Dickinson, Mountain View, CA). Fluorescence
856 intensity was detected by excitation at 644nm and acquisition on the 665/-A channel for

857 MitoTracker Deep Red. ROS measurements were performed as previously described [62]. Briefly,
858 cells were incubated with H_2DCFDA (Molecular Probes) for 30 minutes at 37°C. Cells were
859 trypsinized, washed, and resuspended in 500µl HBSS. Samples were sorted on a BD FACS Canto
860 II system. Fluorescence intensities were calculated by FlowJo (Tree Star, Inc.).
861
862 **Mitochondrial DNA Quantitation**
863 Quantitation of mitochondrial DNA was carried out as previously described [21]. HCT-116 or
864 NT2197 cells were seeded in 6-well dishes for 24 hours. Genomic and mitochondrial DNA were
865 extracted using PureLink Genomic DNA Mini Kit (ThermoFisher) and quantified by qPCR using
866 SensiFAST™ SYBR® Lo-ROX kit (Bioline).
867
868 **Polysome-Profiling Assay**
869 Experiments were carried out as previously described [63]. Briefly, HCT-116 cells were seeded
870 overnight in 150mm plates. The next day, cells were washed in PBS containing 100 µg/ml
871 cycloheximide and lysed in hypotonic buffer (5 mM Tris-HCl [pH 7.5], 2.5 mM $MgCl_2$, 1.5 mM
872 KCl, 100 µg/ml cycloheximide, 2 mM DTT, 0.5% Triton X-100, and 0.5% sodium deoxycholate).
873 Samples were loaded onto 10%-50% wt/vol sucrose density gradients (20 mM HEPES-KOH pH
874 7.6, 100 mM KCl, 5 mM $MgCl_2$) and spun on a SW40Ti rotor (Beckman Coulter) at 4°C (36,000
875 rpm for 2 hours). Samples were fractionated and recorded at OD 254nm using an ISCO fractionator
876 (Teledyne ISCO). RNA from fractions and input was extracted using TRIzol (ThermoFisher)
877 according to the manufacturer's instructions. RNA from each fraction and input was isolated using
878 TRIzol (Invitrogen) according to the manufacturer's instructions. RT-qPCR was performed on

879 fractions and input RNA (refer to section "RNA extraction and RT-qPCR" for more information).
880 Primers are listed in Supplementary Table 2.
881
882 **Puromycilation Assay**
883 HCT-116 cells were grown in 10cm dishes for 24 hours. The next day, cells were treated with
884 puromycin (10ug/ml) for 20 minutes. Cells treated with DMSO were used as negative controls.
885 Cells were lysed and protein samples were quantified. Western blotting was performed (refer to
886 "Western Blotting" section for more information) and membranes were incubated in anti-
887 puromycin antibody (Millipore, Cat#MABE343). Quantification of bands was performed by
888 ImageJ.
889
890 **Stable Isotope Tracing**
891 Metabolite detection by gas chromatography-mass spectrometry (GC-MS) and stable isotope
892 tracing analysis (SITA) was performed as previously described [64]. Briefly, NT2197 cells were
893 seeded in 6-well dishes. Prior to ^{13}C-glutamine SITA experiments, culture media was replaced
894 with one whose composition contains 6mM unlabelled glutamine for 2 hours. Afterwards, media
895 was replaced with media containing 6mM labelled ([U-13C])-glutamine media (Cambridge
896 Isotope Laboratories, MA, USA; CLM-1822; L-glutamine ([U-13C5]), 99%) for 5, 15, 30, and 60
897 minutes. For ^{13}C-leucine SITA experiments, culture media was replaced with one containing
898 unlabelled leucine (0.105g/L) for 2 hours, then incubated in media containing labelled (0.105g/L)
899 ([U-13C])-leucine media (Cambridge Isotope Laboratories, MA, USA; CLM-2262-H-0.1; L-
900 leucine ([U-13C6]), 99%) for 24 hours. Both steady state and tracing samples were washed in cold
901 saline solution (9g/L NaCl) and scraped off with 80% methanol. Samples were sonicated at 4°C

902 for 10 minutes (high setting, 30 seconds on/30 seconds off cycles) to rupture cells. Lysates were
903 centrifuged at 4°C (14000g,10 minutes), and supernatants were collected with addition of an
904 internal standard (750ng myristic acid-D27). Samples were dried overnight at 4°C by speed-vac
905 (Labconco). Dried pellets are resuspended in methoxyamine hydrochloride (10mg/ml), sonicated,
906 and cleared for 10 minutes. Samples are heated 70°C for 30 minutes then applied with N-tert-
907 butyldimethylsilyl-N- methyltrifluoroacetamide (MTBSTFA) at 70°C for 1 hour. Derivatized
908 samples are injected into an Agilent 5975C GC/MS (Agilent Technologies, CA, USA) using
909 methods described previously [64]. ^{13}C-tracer samples were run in parallel with unlabelled samples.
910 MassHunter software (Agilent) was used to carry out mass isotopomer distribution analyses, with
911 metabolites normalized to myristic acid-D27 and cell number. Isotopic distributions were
912 corrected for naturally occurring isotopes using an in-house algorithm [65].
913
914 **Steady-State Analysis of Nucleotides**
915 Steady-state nucleotide abundances were determined using liquid chromatography-mass
916 spectrometry (LC-MS/MS). Cells were washed with 150 mM ammonium formate solution (4°C,
917 pH 7.4), scraped, and extracted with 600µl of methanol/acetonitrile solution (31.6% MeOH/36.3%
918 ACN). Cell lysis and homogenization was conducted by bead-beating with 4 ceramic beads (2
919 mm) for 30 seconds at 50 Hz using a TissueLyser II (Qiagen). Dichloromethane was added to
920 samples, which were subsequently centrifuged to separate extracts into aqueous and organic layers.
921 Supernatants from aqueous layers were dried by vacuum centrifugation at -4°C overnight
922 (Labconco). Dried samples were re-suspended in 50µl of water and centrifuged at 1°C. 5µl of
923 sample was injected onto an Agilent 6470 Triple Quadrupole (QQQ)–LC–MS/MS (Agilent
924 Technologies). Separation of metabolites was conducted using a 1290 Infinity ultra-performance

925 quaternary pump liquid chromatography system, with a mass spectrometer equipped with a Jet
926 Stream™ electrospray ionization source operating in negative mode (Agilent Technologies), with
927 the following settings: source-gas temperature (150 °C), flow (13 L min^{-1}), nebulizer pressure
928 (45 psi), and capillary voltage (2,000 V). Chromatographic resolution of metabolites was
929 conducted using a Zorbax Extend C18 column 1.8 µm, 2.1 × 150mm^2 with guard column 1.8 µm,
930 2.1 × 5mm^2 (Agilent Technologies). The gradient commenced at 100% mobile phase A (97%
931 water, 3% methanol, 10 mM tributylamine, 15 mM acetic acid, 5 µM medronic acid) for 2.5 min,
932 followed with a 5-min gradient to 20% mobile phase C (methanol, 10 mM tributylamine, 15 mM
933 acetic acid, 5 µM medronic acid), a 5.5-min gradient to 45% C and a 7-min gradient to 99% C at
934 a flow rate of 0.25 mL min^{-1}. This was followed by a 4-min hold time at 100% mobile phase C.
935 The column was restored by washing with 99% mobile phase D (90% ACN) for 3 min at 0.25
936 mL min^{-1}, followed by increase of the flow rate to 0.8 mL min^{-1} over 0.5 min and a 3.85-min hold,
937 after which the flow rate was decreased to 0.6 mL min^{-1} over 0.15 min. The column was
938 subsequently re-equilibrated at 100% A over 0.75 min, during which the flow rate was decreased
939 to 0.4 mL min^{-1}, and held for 7.65 min. The flow was brought back to forward flow at 0.25
940 mL min^{-1} one minute before the next injection. The column temperature was maintained at 35°C.
941 Data were analyzed by using MassHunter Quantitative Data Analysis B.10.00 (Agilent
942 Technologies). Data presented are peak area normalized by cell number. Authentic metabolite
943 standards (Sigma Aldrich) were used to obtain reaction monitoring parameters (qualifier/quantifier
944 ions and retention times). All LC/MS grade solvents and salts are purchased from Fisher.
945
946
947

948 **RNA Extraction and RT-qPCR**

949 HCT-116 and NT2197 cells were plated in 6-well dishes and extracted using TRIzol (Ambion) or
950 Aurum Total RNA Mini Kit (Bio-Rad) following the manufacturers' instructions. cDNA was
951 synthesized from purified RNA using SensiFAST cDNA Synthesis Kit (Bioline), as per
952 manufacturer's protocol. RT-qPCR was performed using SensiFAST SYBR Lo-ROX kit
953 (Bioline). Primer sequences are found in Supplementary Table 2.

954

955 **Chromatin Immunopreciptation (ChIP)**

956 Experiments were performed as previously described [44]. Briefly, HCT-116 cells were grown in
957 150mm dishes and fixed in 4% formaldehyde for 10 min, followed by centrifugation. Pellets were
958 resuspended in ChIP-buffer (50 nM Tris (pH 8), 100 mM NaCl, 5 mM EDTA, 1X PMSF, 2 mM
959 NaF, 0.25% NP-40, 0.25% Triton X-100, 0.25% Sodium Deoxycholate, 0.005% SDS)
960 supplemented with 1x cOmplete protease inhibitor (Roche). Samples are sonicated using Sonic
961 Dismembrator Model 500 (ThermoFisher) at 5 cycles at 20% power, 5 cycles at 25% power, 5
962 cycles at 30% power; each cycle is 10 sec. Lysates are spun at 4°C (14,000rpm, 10min) and protein
963 concentration was measured from supernatants using the BCA kit (ThermoFisher). Samples were
964 loaded onto Protein G Plus-Agarose Suspension Beads (Millipore) and pre-cleared at 4°C for 3
965 hours. Input samples were collected, and immunoprecipitation was performed with anti-BCL6
966 (Cell Signaling, #5650) or anti-IgG (Cell Signaling, #2729) on the remainder of the sample
967 overnight at 4°C. The following day, samples were washed in three wash buffers (20 mM Tris
968 (pH 8), 2 mM EDTA, 0.10% SDS, 1% Triton X-100 with 150/200/599mM for Wash1/2/3 buffers
969 respectively), then a wash with LiCl buffer (10 mM Tris (pH 8), 1 mM EDTA, 0.25 M LiCl, 1%
970 NP-40, 1% Sodium Deoxycholate), and two washes with TE buffer (10 mM Tris (pH 8), 1 mM

971 EDTA). Samples were eluted in elution buffer (0.1 M NaHCO3, 1% SDS), and de-crossliked at
972 65°C overnight. The following day, proteinase K was applied to samples and heated at 42°C for 1
973 hour. DNA was purified and collected using DNA collection column (BioBasic). ChIP-qPCR was
974 performed for *EIF4EBP1* and *EIF4EBP2* using sequences found in Supplementary Table 3.
975
976 **Respirometry Assay**
977 Oxygen consumption (OCR) and extracellular acidification rate (ECAR) were measured using
978 Seahorse XFe24 and XFe96 analyzers (Agilent) with the Mito Stress Test (Agilent) and Palmitate
979 Oxidation Assay (Agilent), according to the manufacturer's instructions. Briefly, HCT-116 and
980 NT2197 cells were seeded in Seahorse culture plates (XFe24: 50,000 cells or XFe96: 20,000 cells)
981 and incubated at 37°C. Cells were washed twice and incubated in assay media. For mito stress test
982 experiments, assay media is composed of 10mM glucose, 2mM glutamine, and 1mM sodium
983 pyruvate. Injections include oligomycin (1μM), FCCP (1μM), rotenone/antimycin A (1μM), and
984 monensin (20μM). ATP production from OXPHOS (ATPox) or glycolysis (ATPglyc) were
985 quantified using algorithms presented previously [66]. For palmitate oxidation assay, cells were
986 seeded in substrate-limited media (DMEM, 1% FBS, 0.5mM glucose, 1mM glutamine, 0.5mM
987 carnitine). The next day, cells are washed with FAO Buffer (includes 0.5mM glucose, 0.5mM
988 carnitine, and 5mM HEPES). Immediately prior to run, palmitate-BSA or BSA control is added to
989 the cell media. Basal respiration was recorded and values were normalized to cell counts.
990
991 **Soft Agar/Colony Formation Assay**
992 Experiments were conducted as previously shown [12]. Briefly, 6-well dishes are filled with a bottom
993 layer solution (1:1; 1% noble agar and 2X culture media (2X DMEM, 20% FBS, 2%

994 Pen/Strep/Glutamine)) per well. Dishes are incubated at room temperature for 30 min to allow
995 solution to solidify. 5,000-10,000 HCT-116 and NT2197 cells are mixed 1:1 with 0.6% noble agar
996 and 2X culture media. 1.5ml of this mixture is transferred on top of the solidified agar wells. Dishes
997 are incubated at room temperature to allow the top layer to solidify. Cells are grown at 37°C until
998 colony formation is present. Dishes were stained with nitroblue tetrazolium (Sigma), and colonies
999 were counted.
1000
1001 **Protein Stability Assay**
1002 HCT-116 cells were seeded in 10cm dishes. The next day, cells were treated with cycloheximide
1003 (CHX) (50µg/ml) or DMSO for 2 hours. Furthermore, cells were treated with the proteasomal
1004 inhibitor, MG-132 (10µM) or DMSO for 2 hours. Final time point for all conditions was 4 hours.
1005 Protein was extracted, quantified, and western blotting was performed for ETFDH, p21, 4E-BP1,
1006 or β-actin (refer to "Western Blotting" section for more information).
1007
1008 **RNA Stability Assay**
1009 Assay was performed as previously described [67]. Briefly, HCT-116 cells were seeded in 6-well
1010 dishes. The next day, cells were treated with actinomycinD (ActD) for 2,4,8 and 24 hours. RNA
1011 was extracted, cDNA was synthesized, and RT-qPCR was performed (refer to "RNA extraction
1012 and RT-qPCR" for more information).
1013
1014 **Generation of ETFDH Knockout Cell Lines**
1015 To deplete endogenous ETFDH expression in HCT-116 and NALM6 cells, two guides RNA
1016 (gRNAs) targeting exon 6 and exon 9 of human ETFDH (against ETFDH sequences

1017 AGGTTGGCCGAATGCTAGGATGG and GATGTAGGGATACAAAAGGATGG) (refer to
1018 Supplementary Table 4 for gRNA sequences) were designed using CHOPCHOP
1019 (https://chopchop.cbu.uib.no/)[68] and purchased with the appropriate overhangs to be cloned into
1020 LentiCRISPRv2(GFP) (Addgene #82416). Cloning was carried out as previously described [69,70],
1021 with the following modifications: BsmBI-v2 (New England Biolabs) was used to digest the
1022 lentiCRISPRv2 plasmid; plasmid DNA was recovered using Zymoclean Gel DNA Recovery Kit
1023 (Zymo Research), and ligation was performed overnight at 4°C. Transformation of the ligated
1024 plasmid was carried out at 42°C in chemically competent Stbl3 cells (Fisher Scientific). Bacteria
1025 were plated on Lysogeny Broth (LB)-agar plates containing ampicillin (1 µg/mL) (BioBasic).
1026 Extraction of plasmid DNA was conducted using the QIAprep Spin Miniprep Kit (Qiagen) and
1027 samples were sequenced using primer for human U6 promoter (refer to Supplementary Table 5 for
1028 sequence). Nucleofection was used to deliver the validated lentiCRISPRv2 plasmids into HCT-
1029 116 and NALM6 cells. Transfections of the plasmids were carried out in Nucleofector cuvettes,
1030 according to the optimized protocols for NALM6 and HCT-116 cells (Lonza Bioscience), with
1031 1×10^6 cells used and 1X PBS was used instead of the commercial 4-D Nucleofector solution. Post-
1032 nucleofection, cells were allowed to grow for 72 hours at 37°C, 5% CO_2, prior to cell sorting (BD
1033 FACSAria™ Fusion Flow Cytometer (BD Biosciences)). Cells expressing GFP were selected and
1034 grown in 96-well plates containing conditioned media (45% filtered culture media, 45% fresh
1035 media, & 10% FBS). After two weeks, sorted clones were transferred into 24-well plates and later
1036 into 6-well plates to be collected and validated. Depletion of endogenous ETFDH protein levels in
1037 both HCT-116 and NALM-6 cells was initially confirmed by immunoblotting. Candidate clones
1038 with loss of ETFDH expression were kept for further validation. Moreover, the genomic DNA loci
1039 of candidate clones were sequenced and analyzed for insertion–deletion mutations (INDELs). Two

1040 sets of PCR primers were designed in regions flanking the CRISPR target sites (refer to
1041 Supplementary Table 5 for validation PCR sequences). Extraction of genomic DNA for each clone
1042 was carried out using the PureLink Genomic DNA Mini Kit (Fisher Scientific). Two rounds of
1043 polymerase chain reaction (PCR) on the extracted genomic DNA (35 PCR cycles with Set 1
1044 followed by 45 PCR cycles with Set 2) were carried out and gel electrophoresis was utilized to
1045 separate the PCR products. The smaller PCR product for each clone was excised and purified using
1046 the Zymoclean Gel DNA Recovery Kit (Zymo Research). The products were sequenced, and
1047 chromatograms were analyzed for the presence of mutations causing a premature stop-codon or a
1048 frameshift. Insertion–deletion mutations (INDELs) in *ETFDH* were verified by PCR followed by
1049 sequencing, while the absence of ETFDH protein was confirmed by western blotting for HCT-116
1050 cells and NALM6 cells.

1051 To deplete ETFDH expression in NMuMG, NT2197 and 4T1 cells, two guides (gRNAs)
1052 targeting exon 2 of mouse Etfdh (against mEtfdh sequences 5'-
1053 ATTTTTATGCAGCGTATCACTGG-3' and 5'-GAACATCTTGGAGCACACAGAGG-3')
1054 were designed using CHOPCHOP and cloned in LentiCRISPRv2(GFP) (Addgene #82416) and
1055 sequenced as shown above. For lentiviral production, 2.5×10^5 HEK293T cells were seeded
1056 overnight in a 6-cm dish (Sarstedt). The next day, cells were co-transfected with 4µg of respective
1057 lentiCRISPRV2 GFP plasmid containing either one of the gRNA inserts or empty-lentiCRISPRV2
1058 GFP plasmid, 2.66µg of psPAX2 packaging plasmid (Addgene 35002), and 1.66 µg of pMD2.G
1059 plasmid (Addgene #12259) using the jetPRIME transfection reagent as described by the
1060 manufacturer's protocol (Polyplus transfection). Growth media was changed after 24 hours. After
1061 48 hours, viral supernatant was filtered (0.45 µm filter; (Frogga Bio)), mixed 1:1 with fresh culture
1062 media, and applied to target cells grown in 6-well plates along with 8 µg/mL polybrene (Sigma-

1063 Aldrich). Cells were re-transduced the following two days with viral supernatant. Cells were
1064 allowed to recover for 48 hours post-transduction. Cells were sorted into 96-well plates (Sarstedt)
1065 and grown to generate stable cell lines, as shown above. Depletion of mouse Etfdh protein levels
1066 was initially confirmed via immunoblotting for NT2197, 4T1, and NMuMG. The presence of
1067 INDELs leading to a premature stop codon or frameshift was determined by sequencing as shown
1068 above. Two sets of PCR primers were designed in the regions flanking the CRISPR target sites
1069 (refer to Supplementary Table 5).
1070
1071 **Generation of ETFDH Rescue Cell Lines**
1072 To rescue human ETFDH expression in HCT-116 cells, ETFDH(NM_004453) Human Tagged
1073 ORF was cloned into pLenti-ETFDH-C-Myc-DDK-P2A-Puro plasmid according to the
1074 manufacturer's instructions (Origene) to generate the resulting plasmid, pLenti-ETFDH-C-Myc-
1075 DDK-P2A-Puro. To re-express mutant ETFDH (Y304A, G306E), WT ETFDH, or ORF-Stuffer
1076 lentiviral plasmids conferring hygromycin B resistance were designed using VectorBuilder
1077 (VB250613-1532mdm, VB250613-1530fzr, and VB900172-2887sfj respectively). Plasmids were
1078 transfected with psPAX2, pMD2.G into HEK293T cells with JetPrime reagent (Polyplus)
1079 according to the manufacturer's instructions. Viral supernatants were filtered (0.45µM) and
1080 applied to HCT-116 ETFDH KO cells with polybrene (6µg/mL). After 6 hours, cells were re-
1081 infected overnight. After 2 days, selection with puromycin (4µg/ml) was performed for 72 hours.
1082 Uninfected cells were selected with puromycin to serve as negative controls. The re-introduction
1083 of ETFDH expression or control plasmid in the knockout cells was confirmed via western blotting.
1084 To rescue ETFDH expression in NT2197 ETFDH KO cells, a lentiviral plasmid conferring
1085 hygromycin B resistance and expressing mEtfdh with PAM site mutations or expressing an ORF-

1086 Stuffer was created using VectorBuilder (VB221206-1257xet and VB900123-2599cba
1087 respectively). Lentivirus production and transduction were carried out as previously mentioned for
1088 three consecutive days. After 48h of recovery, cells were selected with 1 mg/mL hygromycin B
1089 for 3 days. Cells were confirmed by western blotting.
1090
1091 **Generation of Poly(A) Track ETFDH Variants**
1092 Mutants were designed by inserting poly(A) tracks of multiple adenosines: control track (CTRL)
1093 [6 consecutive lysine AAG codons $(AAG)_6$], 12 adenosines [12A, equivalent to 4 consecutive
1094 AAA (Lys) codons $(AAA)_4$; 18 adenosines [18A, equivalent to 6 consecutive AAA (Lys) codons
1095 $(AAA)_6$] within the rescue plasmid pLV[Exp]-Hygro-EF1A>mEtfdh. The polyA track insertion
1096 site was determined using AlphaFold (version 2) [37,38] to minimize unintended effects caused by
1097 the poly-lysine stretches on the possible mitochondrial import sequence. The polyA tracks were
1098 inserted following residue 38, in an unstructured loop of the Etfdh protein. Site-directed
1099 mutagenesis was performed using QuikChange II site-directed mutagenesis kit, according to the
1100 manufacturer's instructions (Agilent). Briefly, cycling parameters are followed as: Cycle 1: 95°C
1101 for 1min; Cycle 2: 95°C for 30 sec, 60°C for 30 sec, 68°C for 10min; Cycle 3: 68°C for 7min.
1102 The resulting plasmids were generated: pLV[Exp]-Hygro-EF1A>mEtfdh-AAG_6, pLV[Exp]-
1103 Hygro-EF1A>mEtfdh-AAA_4, pLV[Exp]-Hygro-EF1A>mEtfdh-AAA_6. To generate the poly(A)
1104 track Etfdh mutant lines in NT2197 cells (termed AAG_6, AAA_4, AAA_6), lentivirus production and
1105 transduction into NT2197 ETFDH KO cells was carried out as previously mentioned for three
1106 consecutive days. After 48h of recovery, cells were selected with 1 mg/mL hygromycin B for 3-4
1107 days. ETFDH expression was confirmed by western blotting.
1108

1109 **Generation of Cells Expressing *EIF4EBP1***

1110 pBABE-puro-EV and pBABE-puro-4E-BP1 plasmids were used to overexpress 4E-BP1 in HCT-
1111 116 ETFDH KO cells. Retrovirus production and transduction was carried out similarly to
1112 lentivirus production, except 2.66 µg of pUMVC packaging plasmid (Addgene #8449) was utilized
1113 instead of psPAX2. Following three consecutive days of viral transduction, cells were allowed to
1114 recover for 48h prior to selection with 2 µg/mL puromycin (Sigma-Aldrich) for 3 days. To
1115 overexpress 4e-bp1 in NT2197 ETFDH KO cells, plasmids containing m4e-bp1 or ORF-Stuffer
1116 were generated by VectorBuilder (VB221206-1246sbx & VB900123-2599cba). Lentivirus
1117 production and transduction was carried out as previously mentioned for three consecutive days
1118 prior to a 48h recovery period. After this period, selection with hygromycin B (1 mg/mL) was
1119 conducted for 5-7 days. Validation was observed by western blotting.

1120

1121 **Generation of Knockdown Models by shRNA/siRNA**

1122 Knockdown using shRNA was performed as previously described [20]. For BCL6 knockdown
1123 experiments, the following shRNA vectors were used: pLKO.1 Non-Target shRNA Control
1124 (Sigma, SHC002), BCL6 shRNA #1 (Sigma, TRCN0000084654), or BCL6 shRNA #2
1125 (TRCN0000084655). For RAPTOR/RICTOR knockdown experiments, the following shRNA
1126 vectors were used: scramble shRNA (Addgene, Plasmid #1864), RAPTOR_1 shRNA (Addgene,
1127 Plasmid #1857), and RICTOR_1 shRNA (Addgene, Plasmid #1853). Briefly, HEK293T cells
1128 were transfected with psPAX2, pMD2.G or target pLKO.1 lentiviral shRNA vectors with JetPrime
1129 reagent (Polyplus) according to the manufacturer's instructions. Viral supernatants were filtered
1130 (0.45µM) and transferred to target cells with polybrene (6µg/mL). After 6 hours, cells were re-
1131 infected overnight. After 2 days, selection with puromycin (4µg/ml) was performed for 72 hours.

1132 Uninfected cells were selected with puromycin to serve as negative controls. Cells were seeded
1133 and processed for protein extraction or cell proliferation. Validation was confirmed by western
1134 blotting for *BCL6* knockdown and *RAPTOR* or *RICTOR* knockdown.

1135 Knockdown using siRNA was performed as previously described [64]. Briefly, target cells
1136 were transfected for 24 hours with 50nM Silencer Negative Control No.1 (Thermofisher,
1137 AM4611) or BCL6 siRNA (Thermofisher, Cat#4390771) using JetPrime reagent (Polyplus)
1138 according to the manufacturer's instructions. Cells were re-transfected the next day for 24 hours,
1139 then processed for protein extraction. Validation was confirmed by western blotting.

1140

1141 **Expression Profiles from TCGA/GTEx Databases**

1142 Expression of *ETFDH* and *EIF4EBP1* mRNA across both normal and tumor samples were
1143 obtained from The Cancer Genome Atlas (TCGA) and GTEx repositories. The expression data
1144 were normalized using the TMM (trimmed mean of M values) method and presented as log2
1145 counts per million. Correlations between the genes were assessed using Pearson's correlation
1146 coefficient.

1147

1148 **Quantification and Statistical Analysis**

1149 Statistical analysis was performed using GraphPad Prism 10. Data are presented as mean +/- SD
1150 of independent experiments, unless stated otherwise. Technical replicates were averaged from 2-
1151 3 independent experiments. Details on data quantification, presentation, and statistical analysis are
1152 included in figure legends.

1153

1154

1155 **Data Availability**

1156 Plasmids generated in this study is deposited on Addgene. The original data is available at
1157 Mendeley Data (doi: 10.17632/p4wxkr3vdm.1). Metabolomics data is available at MetaboLights
1158 (MTBLS11048).

1159

1160 **Acknowledgments**

1161 We are thankful to the members of all involved laboratories and Stephane Richard for helpful
1162 discussions. We thank Luc Choinière and Mariana Russo for assistance with metabolomic
1163 experiments, Christian Young for assistance with flow cytometry, and Christopher Rudd for
1164 assistance with respirometry. This research was funded by the Terry Fox Foundation (TFF)
1165 Oncometabolism Team Grant (TFF-242122) to I.T., P.S, and M.P, and Canadian Institutes of
1166 Health Research (CIHR) (PJT-183843, PJT-479494) to I.T. Research in OL's lab is supported by
1167 grants from the Swedish Research Council (2020-01665), Swedish Cancer Society (22 2186), the
1168 Cancer Research Funds of Radiumhemmet (231263) and the Wallenberg Academy Fellow
1169 Program. L-M.P. acknowledges the funds from Queen's University. D.P. is supported by CIHR
1170 Postdoctoral Fellowship (MFE-171312), Cancer Research Society (CRS) The Next Generation of
1171 Scientists Award (NGS), and LDI Desjardins Fellowship Program. P.J. and H.K. are supported by
1172 Fonds de Recherche du Québec – Santé (FRQS) Fellowships. I.T. is supported by Canada Research
1173 Chair in Regulation of mRNA Translation and Metabolism. Metabolic analysis was performed at
1174 the Rosalind and Morris Goodman Cancer Research Centre's Metabolomics Core Facility, which
1175 is supported by the Canada Foundation for Innovation, the Dr. John R. and Clara M. Fraser
1176 Memorial Trust, the Terry Fox Foundation (TFF Oncometabolism Team Grant; TFF-242122), and
1177 McGill University.

1178 **Author Contributions**

1179 Conceptualization, D.P., M.P. and I.T.; Methodology, D.P., R.P., P.J., S.I., H.K., T.B., and S.D.;
1180 Formal Analysis, D.P., P.J., S.T., E.C., S.I., K.J.S. and T.B.; Investigation, D.P., R.P., P.J., S.T.,
1181 E.C., V.S., S.I., S.M., L.Z., H.K., N.C., K.J.S., J.Z., J.V., F.A., and S.M.; Resources, E.G., M.T,
1182 D.A., O.L., L.-M.P., S.D., J.U.-S., P.M.S., M.P., and I.T.; Writing – Original Draft, D.P., M.P.,
1183 and I.T.; Writing – Review & Editing, all authors; Supervision, M.P., and I.T.; Project
1184 Administration, M.P., and I.T.; Funding Acquisition, D.P., M.P., and I.T.

1185

1186 **Competing Interests**

1187 The authors declare no competing interests

1188

1189 **Supplementary Tables**

1190 The online version contains supplementary tables.

1191 Supplementary Table 1: List of Antibodies

1192 Supplementary Table 2: Primer sequences used for RT-qPCR

1193 Supplementary Table 3: Primer sequences used for ChIP-qPCR

1194 Supplementary Table 4: gRNA sequences used for generation of ETFDH KO cell lines

1195 Supplementary Table 5: Primer sequences used for sequencing

1196

1197 **Material & Correspondence**

1198 Further information and requests for reagents may be directed upon reasonable request by the lead
1199 contact, Ivan Topisirovic (ivan.topisirovic@mcgill.ca).

1200

1201 **References**

1202 1 Banerjee, R., Purhonen, J. & Kallijarvi, J. The mitochondrial coenzyme Q junction and
1203 complex III: biochemistry and pathophysiology. *FEBS J* **289**, 6936-6958 (2022).
1204 https://doi.org:10.1111/febs.16164

1205 2 Mereis, M. *et al.* Disorders of flavin adenine dinucleotide metabolism: MADD and related
1206 deficiencies. *Int J Biochem Cell Biol* **132**, 105899 (2021).
1207 https://doi.org:10.1016/j.biocel.2020.105899

1208 3 Ghisla, S. & Thorpe, C. Acyl-CoA dehydrogenases. A mechanistic overview. *Eur J*
1209 *Biochem* **271**, 494-508 (2004). https://doi.org:10.1046/j.1432-1033.2003.03946.x

1210 4 Zhang, Y. *et al.* An acyl-CoA dehydrogenase microplate activity assay using recombinant
1211 porcine electron transfer flavoprotein. *Anal Biochem* **581**, 113332 (2019).
1212 https://doi.org:10.1016/j.ab.2019.06.003

1213 5 El-Gharbawy, A. & Vockley, J. Inborn Errors of Metabolism with Myopathy: Defects of
1214 Fatty Acid Oxidation and the Carnitine Shuttle System. *Pediatr Clin North Am* **65**, 317-
1215 335 (2018). https://doi.org:10.1016/j.pcl.2017.11.006

1216 6 Olsen, R. K. *et al.* ETFDH mutations as a major cause of riboflavin-responsive multiple
1217 acyl-CoA dehydrogenation deficiency. *Brain* **130**, 2045-2054 (2007).
1218 https://doi.org:10.1093/brain/awm135

1219 7 Missaglia, S., Tavian, D. & Angelini, C. ETF dehydrogenase advances in molecular
1220 genetics and impact on treatment. *Crit Rev Biochem Mol Biol* **56**, 360-372 (2021).
1221 https://doi.org:10.1080/10409238.2021.1908952

1222 8 Herrero Martin, J. C. *et al.* An ETFDH-driven metabolon supports OXPHOS efficiency in
1223 skeletal muscle by regulating coenzyme Q homeostasis. *Nat Metab* **6**, 209-225 (2024).
1224 https://doi.org:10.1038/s42255-023-00956-y
1225 9 Bertomeu, T. *et al.* A High-Resolution Genome-Wide CRISPR/Cas9 Viability Screen
1226 Reveals Structural Features and Contextual Diversity of the Human Cell-Essential
1227 Proteome. *Mol Cell Biol* **38** (2018). https://doi.org:10.1128/MCB.00302-17
1228 10 Tsherniak, A. *et al.* Defining a Cancer Dependency Map. *Cell* **170**, 564-576 e516 (2017).
1229 https://doi.org:10.1016/j.cell.2017.06.010
1230 11 Ursini-Siegel, J. *et al.* ShcA signalling is essential for tumour progression in mouse models
1231 of human breast cancer. *EMBO J* **27**, 910-920 (2008).
1232 https://doi.org:10.1038/emboj.2008.22
1233 12 Borowicz, S. *et al.* The soft agar colony formation assay. *J Vis Exp*, e51998 (2014).
1234 https://doi.org:10.3791/51998
1235 13 DeBerardinis, R. J. & Cheng, T. Q's next: the diverse functions of glutamine in metabolism,
1236 cell biology and cancer. *Oncogene* **29**, 313-324 (2010).
1237 https://doi.org:10.1038/onc.2009.358
1238 14 Saxton, R. A. & Sabatini, D. M. mTOR Signaling in Growth, Metabolism, and Disease.
1239 *Cell* **168**, 960-976 (2017). https://doi.org:10.1016/j.cell.2017.02.004
1240 15 Thoreen, C. C. *et al.* An ATP-competitive mammalian target of rapamycin inhibitor reveals
1241 rapamycin-resistant functions of mTORC1. *J Biol Chem* **284**, 8023-8032 (2009).
1242 https://doi.org:10.1074/jbc.M900301200

1243 16 Lee, B. J. *et al.* Selective inhibitors of mTORC1 activate 4EBP1 and suppress tumor
1244 growth. *Nat Chem Biol* **17**, 1065-1074 (2021). https://doi.org:10.1038/s41589-021-00813-
1245 7
1246 17 Harding, H. P. *et al.* Regulated translation initiation controls stress-induced gene
1247 expression in mammalian cells. *Mol Cell* **6**, 1099-1108 (2000).
1248 https://doi.org:10.1016/s1097-2765(00)00108-8
1249 18 Dowling, R. J. *et al.* mTORC1-mediated cell proliferation, but not cell growth, controlled
1250 by the 4E-BPs. *Science* **328**, 1172-1176 (2010). https://doi.org:10.1126/science.1187532
1251 19 Gingras, A. C. *et al.* Regulation of 4E-BP1 phosphorylation: a novel two-step mechanism.
1252 *Genes Dev* **13**, 1422-1437 (1999). https://doi.org:10.1101/gad.13.11.1422
1253 20 Hulea, L. *et al.* Translational and HIF-1alpha-Dependent Metabolic Reprogramming
1254 Underpin Metabolic Plasticity and Responses to Kinase Inhibitors and Biguanides. *Cell*
1255 *Metab* **28**, 817-832 e818 (2018). https://doi.org:10.1016/j.cmet.2018.09.001
1256 21 Morita, M. *et al.* mTORC1 controls mitochondrial activity and biogenesis through 4E-BP-
1257 dependent translational regulation. *Cell Metab* **18**, 698-711 (2013).
1258 https://doi.org:10.1016/j.cmet.2013.10.001
1259 22 Morita, M. *et al.* mTOR coordinates protein synthesis, mitochondrial activity and
1260 proliferation. *Cell Cycle* **14**, 473-480 (2015).
1261 https://doi.org:10.4161/15384101.2014.991572
1262 23 Yamaguchi, S. *et al.* ATF4-mediated induction of 4E-BP1 contributes to pancreatic beta
1263 cell survival under endoplasmic reticulum stress. *Cell Metab* **7**, 269-276 (2008).
1264 https://doi.org:10.1016/j.cmet.2008.01.008

1265 24 Wang, J. *et al.* Snail determines the therapeutic response to mTOR kinase inhibitors by
1266 transcriptional repression of 4E-BP1. *Nat Commun* **8**, 2207 (2017).
1267 https://doi.org:10.1038/s41467-017-02243-3
1268 25 Totten, S. P. *et al.* STAT1 potentiates oxidative stress revealing a targetable vulnerability
1269 that increases phenformin efficacy in breast cancer. *Nat Commun* **12**, 3299 (2021).
1270 https://doi.org:10.1038/s41467-021-23396-2
1271 26 Hayes, J. D., Dinkova-Kostova, A. T. & Tew, K. D. Oxidative Stress in Cancer. *Cancer*
1272 *Cell* **38**, 167-197 (2020). https://doi.org:10.1016/j.ccell.2020.06.001
1273 27 Nakayamada, S. *et al.* Type I IFN induces binding of STAT1 to Bcl6: divergent roles of
1274 STAT family transcription factors in the T follicular helper cell genetic program. *J*
1275 *Immunol* **192**, 2156-2166 (2014). https://doi.org:10.4049/jimmunol.1300675
1276 28 Liu, Y. *et al.* The oncoprotein BCL6 enables solid tumor cells to evade genotoxic stress.
1277 *Elife* **11** (2022). https://doi.org:10.7554/eLife.69255
1278 29 Madapura, H. S. *et al.* Interferon gamma is a STAT1-dependent direct inducer of BCL6
1279 expression in imatinib-treated chronic myeloid leukemia cells. *Oncogene* **36**, 4619-4628
1280 (2017). https://doi.org:10.1038/onc.2017.85
1281 30 Ramachandran, K. *et al.* Transcriptional programming of translation by BCL6 controls
1282 skeletal muscle proteostasis. *Nat Metab* **6**, 304-322 (2024).
1283 https://doi.org:10.1038/s42255-024-00983-3
1284 31 Yi, W. *et al.* The mTORC1-4E-BP-eIF4E axis controls de novo Bcl6 protein synthesis in
1285 T cells and systemic autoimmunity. *Nat Commun* **8**, 254 (2017).
1286 https://doi.org:10.1038/s41467-017-00348-3

1287 32 Xu, L. *et al.* The Kinase mTORC1 Promotes the Generation and Suppressive Function of
1288 Follicular Regulatory T Cells. *Immunity* **47**, 538-551 e535 (2017).
1289 https://doi.org:10.1016/j.immuni.2017.08.011
1290 33 Raybuck, A. L. *et al.* B Cell-Intrinsic mTORC1 Promotes Germinal Center-Defining
1291 Transcription Factor Gene Expression, Somatic Hypermutation, and Memory B Cell
1292 Generation in Humoral Immunity. *J Immunol* **200**, 2627-2639 (2018).
1293 https://doi.org:10.4049/jimmunol.1701321
1294 34 Consortium, I. T. P.-C. A. o. W. G. Pan-cancer analysis of whole genomes. *Nature* **578**,
1295 82-93 (2020). https://doi.org:10.1038/s41586-020-1969-6
1296 35 Powell, G., Pavlovic Djuranovic, S. & Djuranovic, S. Gene dosage effects of poly(A) track-
1297 engineered hypomorphs. *Mol Ther Nucleic Acids* **26**, 865-878 (2021).
1298 https://doi.org:10.1016/j.omtn.2021.10.005
1299 36 Arthur, L. *et al.* Translational control by lysine-encoding A-rich sequences. *Sci Adv* **1**
1300 (2015). https://doi.org:10.1126/sciadv.1500154
1301 37 Jumper, J. *et al.* Highly accurate protein structure prediction with AlphaFold. *Nature* **596**,
1302 583-589 (2021). https://doi.org:10.1038/s41586-021-03819-2
1303 38 Varadi, M. *et al.* AlphaFold Protein Structure Database: massively expanding the structural
1304 coverage of protein-sequence space with high-accuracy models. *Nucleic Acids Res* **50**,
1305 D439-D444 (2022). https://doi.org:10.1093/nar/gkab1061
1306 39 Jones, P. A. & Baylin, S. B. The fundamental role of epigenetic events in cancer. *Nat Rev*
1307 *Genet* **3**, 415-428 (2002). https://doi.org:10.1038/nrg816

1308 40 Nilsson, R. *et al.* Metabolic enzyme expression highlights a key role for MTHFD2 and the
1309 mitochondrial folate pathway in cancer. *Nat Commun* **5**, 3128 (2014).
1310 https://doi.org:10.1038/ncomms4128
1311 41 Smith, H. W. *et al.* An ErbB2/c-Src axis links bioenergetics with PRC2 translation to drive
1312 epigenetic reprogramming and mammary tumorigenesis. *Nat Commun* **10**, 2901 (2019).
1313 https://doi.org:10.1038/s41467-019-10681-4
1314 42 Harachi, M. *et al.* Dual Regulation of Histone Methylation by mTOR Complexes Controls
1315 Glioblastoma Tumor Cell Growth via EZH2 and SAM. *Mol Cancer Res* **18**, 1142-1152
1316 (2020). https://doi.org:10.1158/1541-7786.MCR-20-0024
1317 43 Chen, M. *et al.* The activation of mTOR signalling modulates DNA methylation by
1318 enhancing DNMT1 translation in hepatocellular carcinoma. *J Transl Med* **21**, 276 (2023).
1319 https://doi.org:10.1186/s12967-023-04103-9
1320 44 Kim, H. *et al.* MTOR modulation induces selective perturbations in histone methylation
1321 which influence the anti-proliferative effects of mTOR inhibitors. *iScience* **27**, 109188
1322 (2024). https://doi.org:10.1016/j.isci.2024.109188
1323 45 Petroulakis, E. *et al.* p53-dependent translational control of senescence and transformation
1324 via 4E-BPs. *Cancer Cell* **16**, 439-446 (2009). https://doi.org:10.1016/j.ccr.2009.09.025
1325 46 Hsieh, A. C. *et al.* Genetic dissection of the oncogenic mTOR pathway reveals druggable
1326 addiction to translational control via 4EBP-eIF4E. *Cancer Cell* **17**, 249-261 (2010).
1327 https://doi.org:10.1016/j.ccr.2010.01.021
1328 47 Polunovsky, V. A. *et al.* Translational control of the antiapoptotic function of Ras. *J Biol*
1329 *Chem* **275**, 24776-24780 (2000). https://doi.org:10.1074/jbc.M001938200

1330 48 Lynch, M., Fitzgerald, C., Johnston, K. A., Wang, S. & Schmidt, E. V. Activated eIF4E-
1331 binding protein slows G1 progression and blocks transformation by c-myc without
1332 inhibiting cell growth. *J Biol Chem* **279**, 3327-3339 (2004).
1333 https://doi.org:10.1074/jbc.M310872200
1334 49 Avdulov, S. *et al.* Activation of translation complex eIF4F is essential for the genesis and
1335 maintenance of the malignant phenotype in human mammary epithelial cells. *Cancer Cell*
1336 **5**, 553-563 (2004). https://doi.org:10.1016/j.ccr.2004.05.024
1337 50 Rousseau, D., Gingras, A. C., Pause, A. & Sonenberg, N. The eIF4E-binding proteins 1
1338 and 2 are negative regulators of cell growth. *Oncogene* **13**, 2415-2420 (1996).
1339 51 Musa, J. *et al.* Eukaryotic initiation factor 4E-binding protein 1 (4E-BP1): a master
1340 regulator of mRNA translation involved in tumorigenesis. *Oncogene* **35**, 4675-4688
1341 (2016). https://doi.org:10.1038/onc.2015.515
1342 52 Jewer, M. *et al.* Translational control of breast cancer plasticity. *Nat Commun* **11**, 2498
1343 (2020). https://doi.org:10.1038/s41467-020-16352-z
1344 53 Teleman, A. A., Chen, Y. W. & Cohen, S. M. 4E-BP functions as a metabolic brake used
1345 under stress conditions but not during normal growth. *Genes Dev* **19**, 1844-1848 (2005).
1346 https://doi.org:10.1101/gad.341505
1347 54 Levy, T. *et al.* mTORC1 regulates cell survival under glucose starvation through 4EBP1/2-
1348 mediated translational reprogramming of fatty acid metabolism. *Nat Commun* **15**, 4083
1349 (2024). https://doi.org:10.1038/s41467-024-48386-y
1350 55 Valenstein, M. L. *et al.* Structural basis for the dynamic regulation of mTORC1 by amino
1351 acids. *Nature* **646**, 493-500 (2025). https://doi.org:10.1038/s41586-025-09428-7

1352 56 Appuhamy, J. A., Knoebel, N. A., Nayananjalie, W. A., Escobar, J. & Hanigan, M. D.
1353 Isoleucine and leucine independently regulate mTOR signaling and protein synthesis in
1354 MAC-T cells and bovine mammary tissue slices. *J Nutr* **142**, 484-491 (2012).
1355 https://doi.org:10.3945/jn.111.152595
1356 57 Herningtyas, E. H. *et al.* Branched-chain amino acids and arginine suppress
1357 MaFbx/atrogin-1 mRNA expression via mTOR pathway in C2C12 cell line. *Biochim*
1358 *Biophys Acta* **1780**, 1115-1120 (2008). https://doi.org:10.1016/j.bbagen.2008.06.004
1359 58 Jewell, J. L. *et al.* Metabolism. Differential regulation of mTORC1 by leucine and
1360 glutamine. *Science* **347**, 194-198 (2015). https://doi.org:10.1126/science.1259472
1361 59 Tan, H. W. S., Sim, A. Y. L. & Long, Y. C. Glutamine metabolism regulates autophagy-
1362 dependent mTORC1 reactivation during amino acid starvation. *Nat Commun* **8**, 338
1363 (2017). https://doi.org:10.1038/s41467-017-00369-y
1364 60 Chen, R. *et al.* The general amino acid control pathway regulates mTOR and autophagy
1365 during serum/glutamine starvation. *J Cell Biol* **206**, 173-182 (2014).
1366 https://doi.org:10.1083/jcb.201403009
1367 61 Tabaries, S. *et al.* Claudin-2 promotes colorectal cancer liver metastasis and is a biomarker
1368 of the replacement type growth pattern. *Commun Biol* **4**, 657 (2021).
1369 https://doi.org:10.1038/s42003-021-02189-9
1370 62 Igelmann, S. *et al.* A hydride transfer complex reprograms NAD metabolism and bypasses
1371 senescence. *Mol Cell* **81**, 3848-3865 e3819 (2021).
1372 https://doi.org:10.1016/j.molcel.2021.08.028
1373 63 Gandin, V. *et al.* Polysome fractionation and analysis of mammalian translatomes on a
1374 genome-wide scale. *J Vis Exp* (2014). https://doi.org:10.3791/51455

1375 64 Papadopoli, D. *et al.* Perturbations of cancer cell metabolism by the antidiabetic drug
1376 canagliflozin. *Neoplasia* **23**, 391-399 (2021). https://doi.org:10.1016/j.neo.2021.02.003
1377 65 McGuirk, S. *et al.* PGC-1alpha supports glutamine metabolism in breast cancer. *Cancer*
1378 *Metab* **1**, 22 (2013). https://doi.org:10.1186/2049-3002-1-22
1379 66 Mookerjee, S. A., Gerencser, A. A., Nicholls, D. G. & Brand, M. D. Quantifying
1380 intracellular rates of glycolytic and oxidative ATP production and consumption using
1381 extracellular flux measurements. *J Biol Chem* **292**, 7189-7207 (2017).
1382 https://doi.org:10.1074/jbc.M116.774471
1383 67 Topisirovic, I. *et al.* Stability of eukaryotic translation initiation factor 4E mRNA is
1384 regulated by HuR, and this activity is dysregulated in cancer. *Mol Cell Biol* **29**, 1152-1162
1385 (2009). https://doi.org:10.1128/MCB.01532-08
1386 68 Labun, K. *et al.* CHOPCHOP v3: expanding the CRISPR web toolbox beyond genome
1387 editing. *Nucleic Acids Res* **47**, W171-W174 (2019). https://doi.org:10.1093/nar/gkz365
1388 69 Sanjana, N. E., Shalem, O. & Zhang, F. Improved vectors and genome-wide libraries for
1389 CRISPR screening. *Nat Methods* **11**, 783-784 (2014). https://doi.org:10.1038/nmeth.3047
1390 70 Shalem, O. *et al.* Genome-scale CRISPR-Cas9 knockout screening in human cells. *Science*
1391 **343**, 84-87 (2014). https://doi.org:10.1126/science.1247005
1392

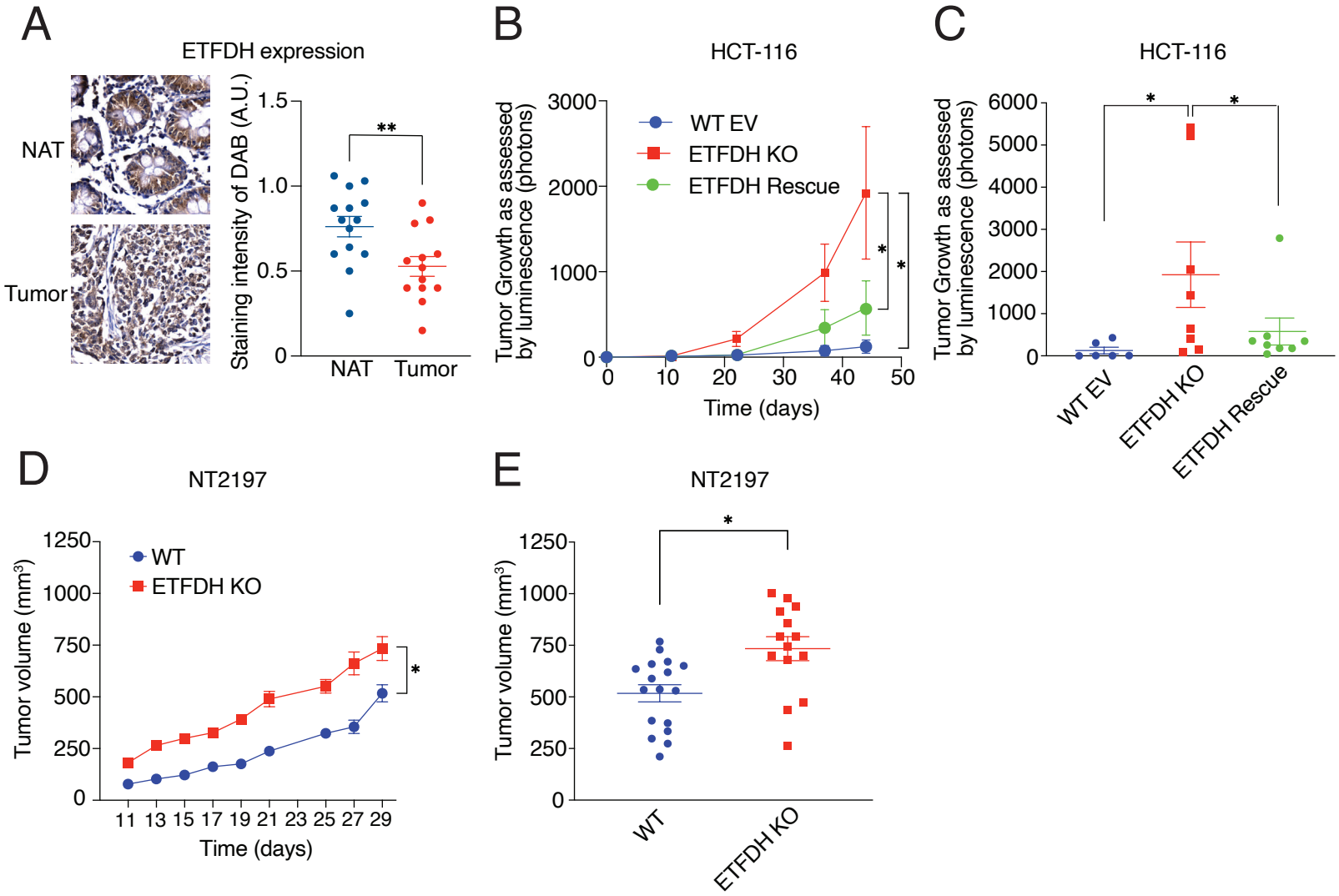
A
ETFDH expression
NAT
Tumor
Staining intensity of DAB (A.U.)
1.5
1.0
0.5
0
**
NAT
Tumor
B
HCT-116
Tumor Growth as assessed by luminescence (photons)
3000
2000
1000
0
WT EV
ETFDH KO
ETFDH Rescue
*
*
0
10
20
30
40
50
Time (days)
C
HCT-116
Tumor Growth as assessed by luminescence (photons)
6000
5000
4000
3000
2000
1000
0
*
*
WT EV
ETFDH KO
ETFDH Rescue
D
NT2197
Tumor volume (mm3)
1250
1000
750
500
250
0
WT
ETFDH KO
*
11 13 15 17 19 21 23 25 27 29
Time (days)
E
NT2197
Tumor volume (mm3)
1250
1000
750
500
250
0
*
WT
ETFDH KO

Fig.1

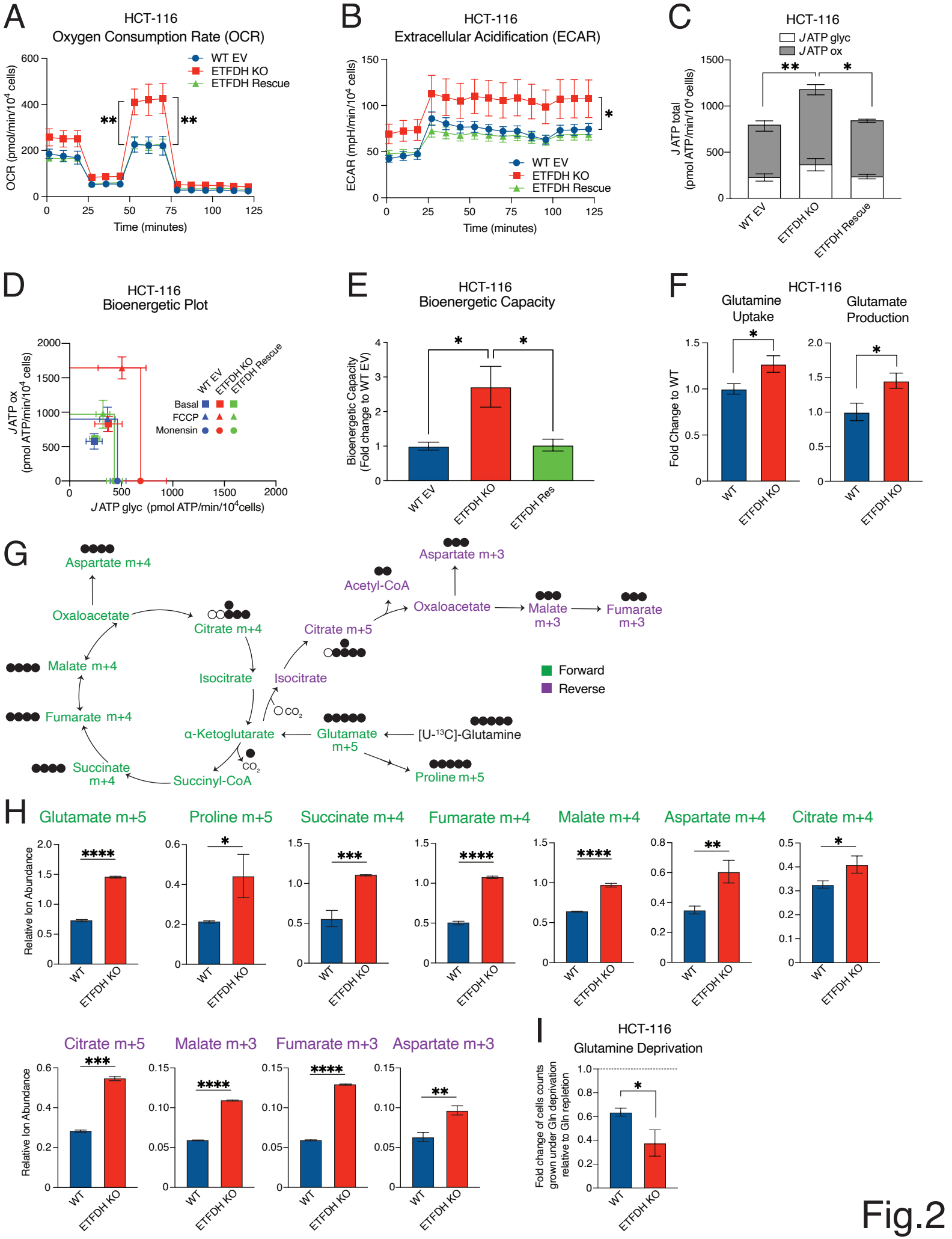
A
HCT-116
Oxygen Consumption Rate (OCR)
WT EV
ETFDH KO
ETFDH Rescue
OCR (pmol/min/10^4 cells)
Time (minutes)
B
HCT-116
Extracellular Acidification (ECAR)
ECAR (mpH/min/10^4 cells)
Time (minutes)
C
HCT-116
J ATP glyc
J ATP ox
J ATP total (pmol ATP/min/10^4 cells)
WT EV
ETFDH KO
ETFDH Rescue
D
HCT-116
Bioenergetic Plot
J ATP ox (pmol ATP/min/10^4 cells)
J ATP glyc (pmol ATP/min/10^4 cells)
Basal
FCCP
Monensin
E
HCT-116
Bioenergetic Capacity
Bioenergetic Capacity (Fold change to WT EV)
WT EV
ETFDH KO
ETFDH Res
F
HCT-116
Glutamine Uptake
Glutamate Production
Fold Change to WT
WT
ETFDH KO
G
Aspartate m+4
Oxaloacetate
Citrate m+4
Malate m+4
Isocitrate
Fumarate m+4
α-Ketoglutarate
Succinate m+4
Succinyl-CoA
Citrate m+5
Isocitrate
Acetyl-CoA
Aspartate m+3
Oxaloacetate
Malate m+3
Fumarate m+3
Glutamate m+5
[U-13C]-Glutamine
Proline m+5
Forward
Reverse
H
Glutamate m+5
Proline m+5
Succinate m+4
Fumarate m+4
Malate m+4
Aspartate m+4
Citrate m+4
Citrate m+5
Malate m+3
Fumarate m+3
Aspartate m+3
Relative Ion Abundance
WT
ETFDH KO
I
HCT-116
Glutamine Deprivation
Fold change of cells counts grown under Gln deprivation relative to Gln repletion
WT
ETFDH KO

Fig.2

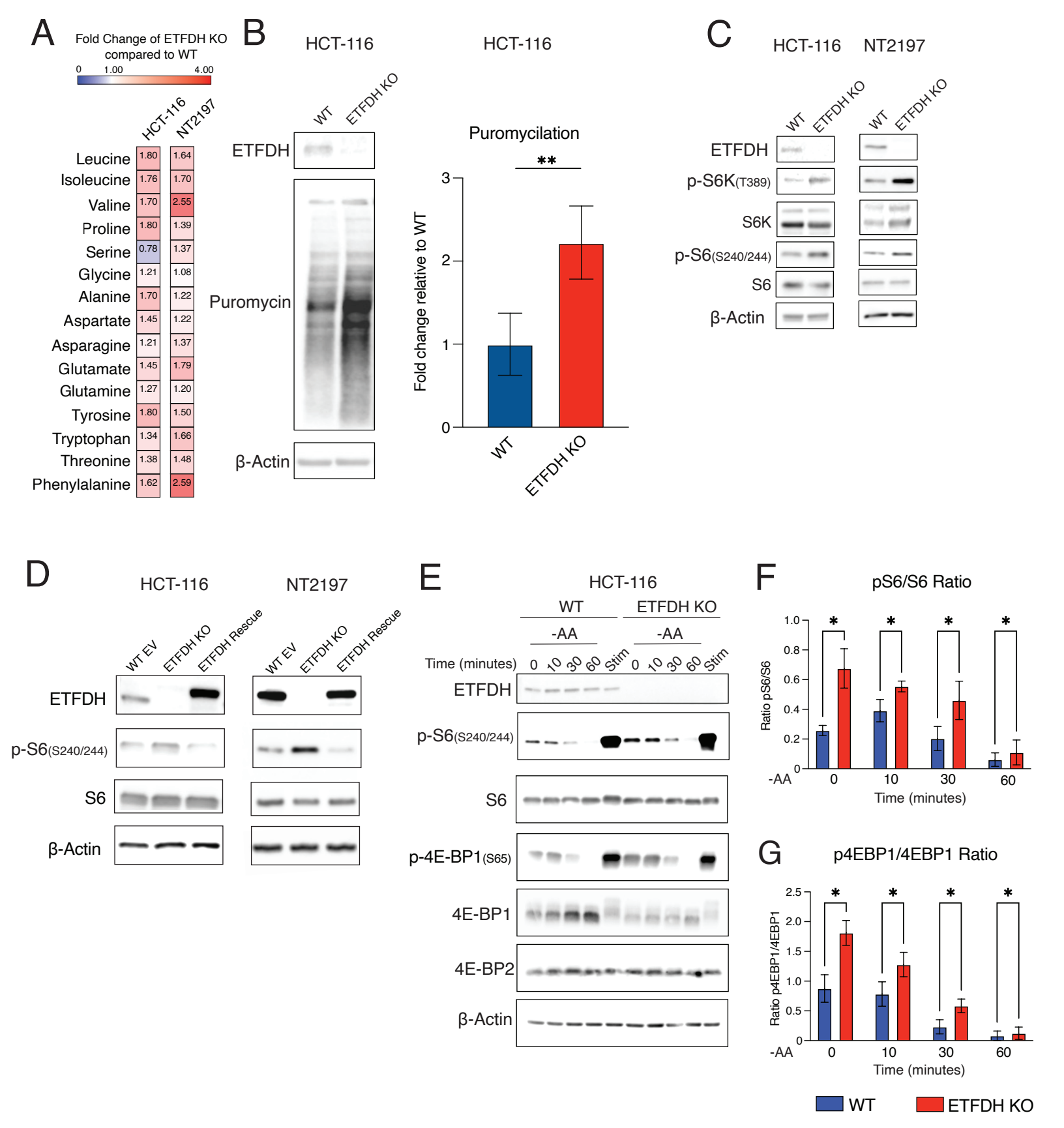
A
Fold Change of ETFDH KO compared to WT
0
1.00
4.00
HCT-116
NT2197
Leucine 1.80 1.64
Isoleucine 1.76 1.70
Valine 1.70 2.55
Proline 1.80 1.39
Serine 0.78 1.37
Glycine 1.21 1.08
Alanine 1.70 1.22
Aspartate 1.45 1.22
Asparagine 1.21 1.37
Glutamate 1.45 1.79
Glutamine 1.27 1.20
Tyrosine 1.80 1.50
Tryptophan 1.34 1.66
Threonine 1.38 1.48
Phenylalanine 1.62 2.59
B
HCT-116
WT
ETFDH KO
ETFDH
Puromycin
β-Actin
HCT-116
Puromycilation
**
Fold change relative to WT
0
1
2
3
WT
ETFDH KO
C
HCT-116
NT2197
WT
ETFDH KO
WT
ETFDH KO
ETFDH
p-S6K(T389)
S6K
p-S6(S240/244)
S6
β-Actin
D
HCT-116
NT2197
WT EV
ETFDH KO
ETFDH Rescue
WT EV
ETFDH KO
ETFDH Rescue
ETFDH
p-S6(S240/244)
S6
β-Actin
E
HCT-116
WT
ETFDH KO
-AA
-AA
Time (minutes)
0
10
30
60
Stim
0
10
30
60
Stim
ETFDH
p-S6(S240/244)
S6
p-4E-BP1(S65)
4E-BP1
4E-BP2
β-Actin
F
pS6/S6 Ratio
Ratio pS6/S6
0
0.2
0.4
0.6
0.8
1.0
*
*
*
*
-AA
0
10
30
60
Time (minutes)
G
p4EBP1/4EBP1 Ratio
Ratio p4EBP1/4EBP1
0
0.5
1.0
1.5
2.0
2.5
*
*
*
*
-AA
0
10
30
60
Time (minutes)
WT
ETFDH KO

Fig.3

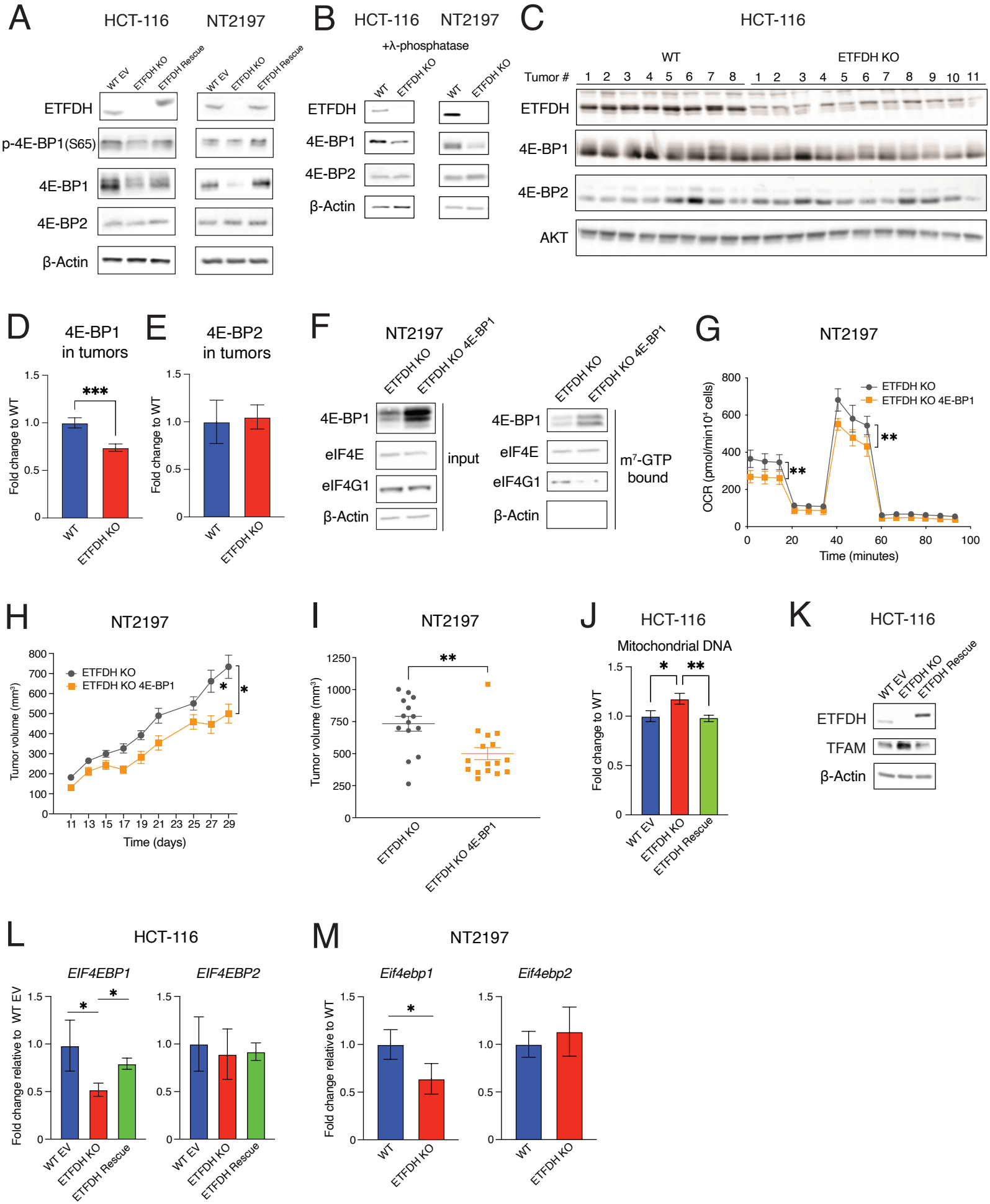
A
HCT-116
NT2197
WT EV
ETFDH KO
ETFDH Rescue
ETFDH
p-4E-BP1(S65)
4E-BP1
4E-BP2
β-Actin
B
HCT-116
NT2197
+λ-phosphatase
WT
ETFDH KO
ETFDH
4E-BP1
4E-BP2
β-Actin
C
HCT-116
WT
ETFDH KO
Tumor #
1 2 3 4 5 6 7 8
1 2 3 4 5 6 7 8 9 10 11
ETFDH
4E-BP1
4E-BP2
AKT
D
4E-BP1
in tumors
Fold change to WT
***
WT
ETFDH KO
E
4E-BP2
in tumors
Fold change to WT
WT
ETFDH KO
F
NT2197
ETFDH KO
ETFDH KO 4E-BP1
4E-BP1
eIF4E
eIF4G1
β-Actin
input
m7-GTP
bound
G
NT2197
ETFDH KO
ETFDH KO 4E-BP1
OCR (pmol/min10⁴ cells)
Time (minutes)
**
H
NT2197
ETFDH KO
ETFDH KO 4E-BP1
Tumor volume (mm³)
Time (days)
*
I
NT2197
Tumor volume (mm³)
**
ETFDH KO
ETFDH KO 4E-BP1
J
HCT-116
Mitochondrial DNA
Fold change to WT
*
**
WT EV
ETFDH KO
ETFDH Rescue
K
HCT-116
WT EV
ETFDH KO
ETFDH Rescue
ETFDH
TFAM
β-Actin
L
HCT-116
EIF4EBP1
EIF4EBP2
Fold change relative to WT EV
*
WT EV
ETFDH KO
ETFDH Rescue
M
NT2197
Eif4ebp1
Eif4ebp2
Fold change relative to WT
*
WT
ETFDH KO

Fig.4

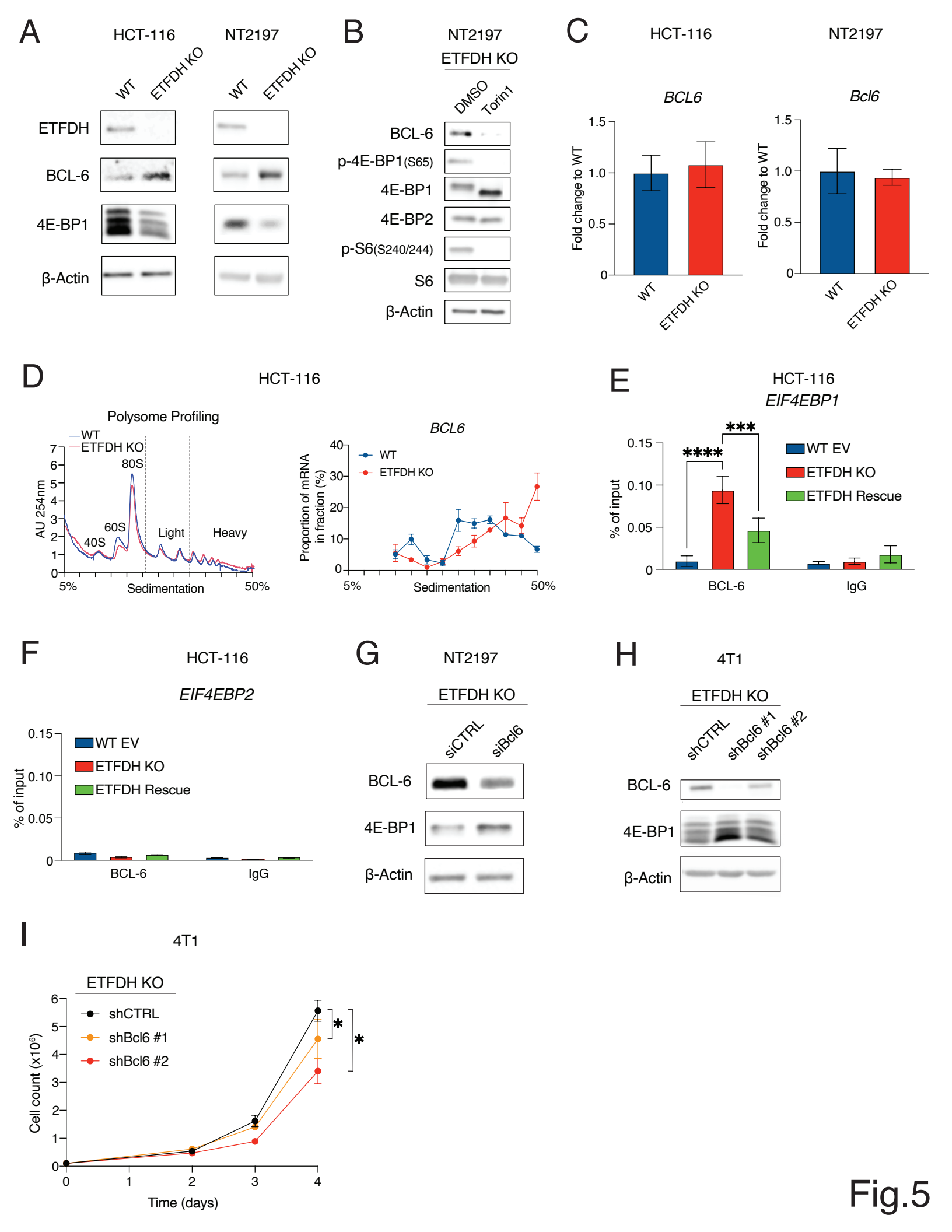
A
HCT-116
NT2197
WT
ETFDH KO
WT
ETFDH KO
ETFDH
BCL-6
4E-BP1
β-Actin
B
NT2197
ETFDH KO
DMSO
Torin1
BCL-6
p-4E-BP1(S65)
4E-BP1
4E-BP2
p-S6(S240/244)
S6
β-Actin
C
HCT-116
NT2197
BCL6
Bcl6
Fold change to WT
1.5
1.0
0.5
0
WT
ETFDH KO
D
HCT-116
Polysome Profiling
WT
ETFDH KO
AU 254nm
80S
60S
40S
Light
Heavy
5%
Sedimentation
50%
BCL6
Proportion of mRNA in fraction (%)
40
30
20
10
0
WT
ETFDH KO
5%
Sedimentation
50%
E
HCT-116
EIF4EBP1
% of input
0.15
0.10
0.05
0
****
***
WT EV
ETFDH KO
ETFDH Rescue
BCL-6
IgG
F
HCT-116
EIF4EBP2
% of input
0.15
0.10
0.05
0
WT EV
ETFDH KO
ETFDH Rescue
BCL-6
IgG
G
NT2197
ETFDH KO
siCTRL
siBcl6
BCL-6
4E-BP1
β-Actin
H
4T1
ETFDH KO
shCTRL
shBcl6 #1
shBcl6 #2
BCL-6
4E-BP1
β-Actin
I
4T1
ETFDH KO
shCTRL
shBcl6 #1
shBcl6 #2
Cell count (x10⁶)
6
5
4
3
2
1
0
*
*
0
1
2
3
4
Time (days)

Fig.5

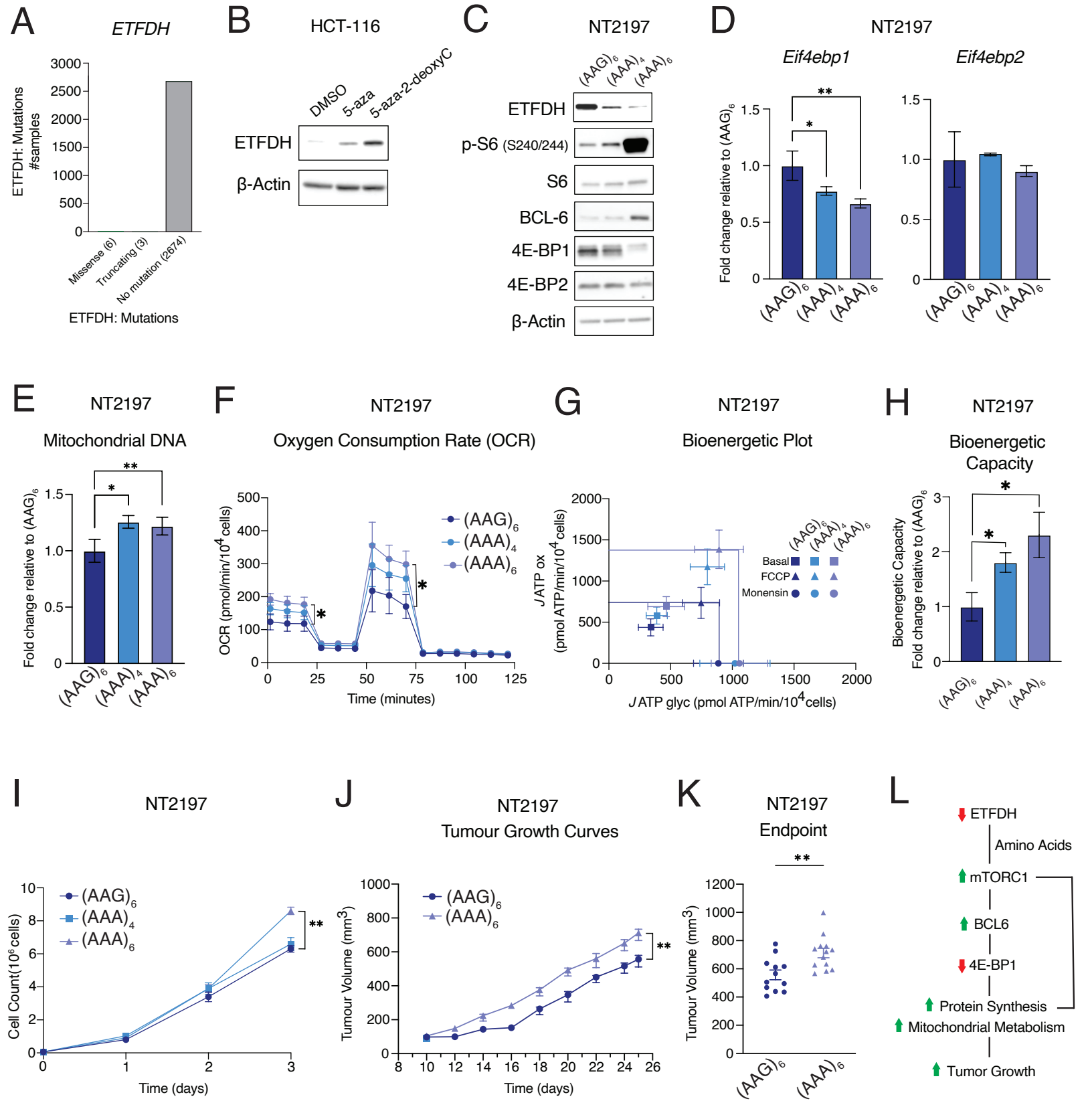
A
ETFDH
ETFDH: Mutations #samples
3000
2500
2000
1500
1000
500
0
Missense (6)
Truncating (3)
No mutation (2674)
ETFDH: Mutations
B
HCT-116
DMSO
5-aza
5-aza-2-deoxyC
ETFDH
β-Actin
C
NT2197
(AAG)6
(AAA)4
(AAA)6
ETFDH
p-S6 (S240/244)
S6
BCL-6
4E-BP1
4E-BP2
β-Actin
D
NT2197
Eif4ebp1
Eif4ebp2
Fold change relative to (AAG)6
E
NT2197
Mitochondrial DNA
Fold change relative to (AAG)6
F
NT2197
Oxygen Consumption Rate (OCR)
OCR (pmol/min/10^4 cells)
Time (minutes)
G
NT2197
Bioenergetic Plot
J ATP ox (pmol ATP/min/10^4 cells)
J ATP glyc (pmol ATP/min/10^4 cells)
Basal
FCCP
Monensin
H
NT2197
Bioenergetic Capacity
Bioenergetic Capacity
Fold change relative to (AAG)6
I
NT2197
Cell Count(10^6 cells)
Time (days)
J
NT2197
Tumour Growth Curves
Tumour Volume (mm^3)
Time (days)
K
NT2197
Endpoint
Tumour Volume (mm^3)
L
ETFDH
Amino Acids
mTORC1
BCL6
4E-BP1
Protein Synthesis
Mitochondrial Metabolism
Tumor Growth

Fig.6

Supplementary Figure 1

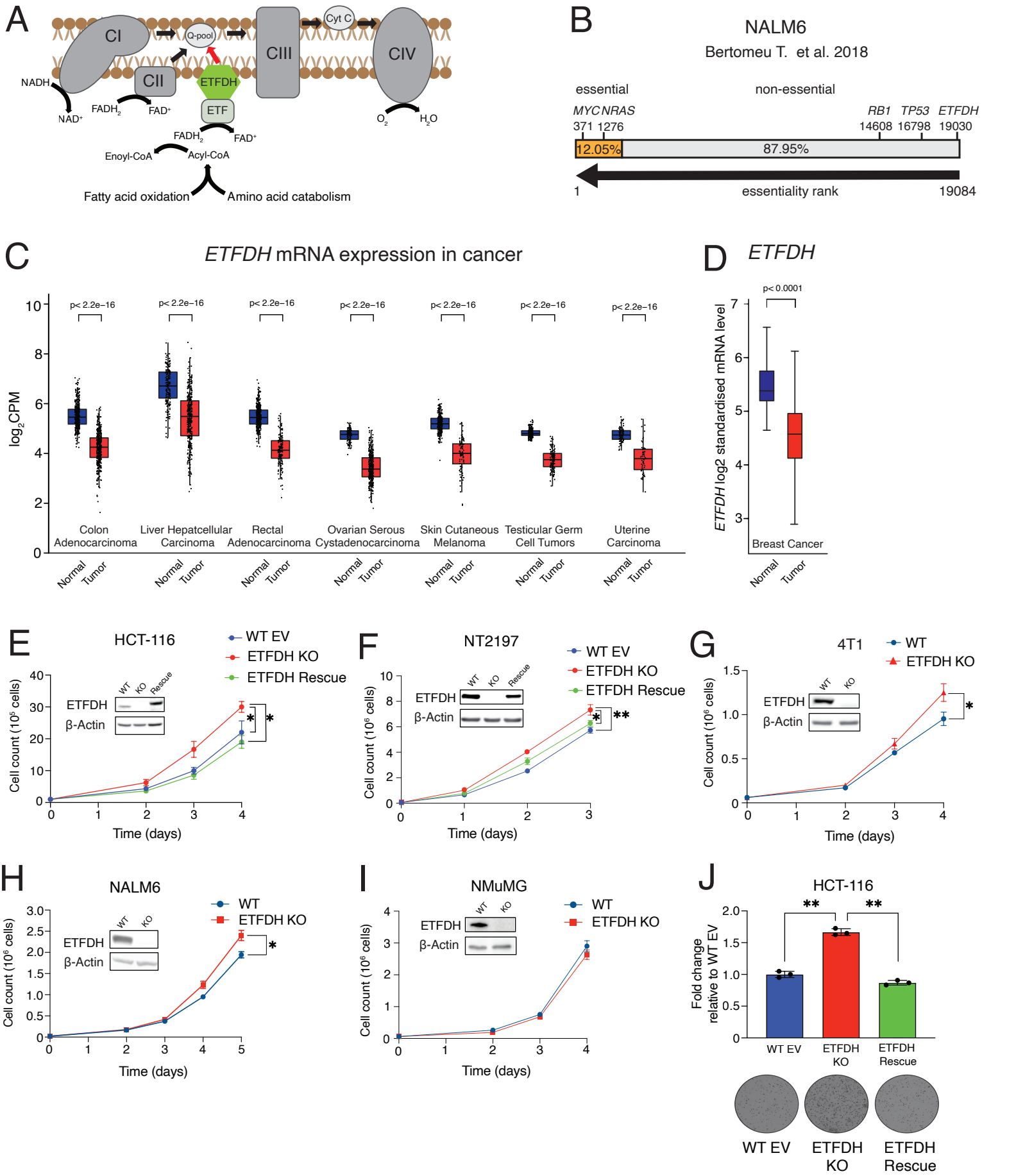

Supplementary Figure 2

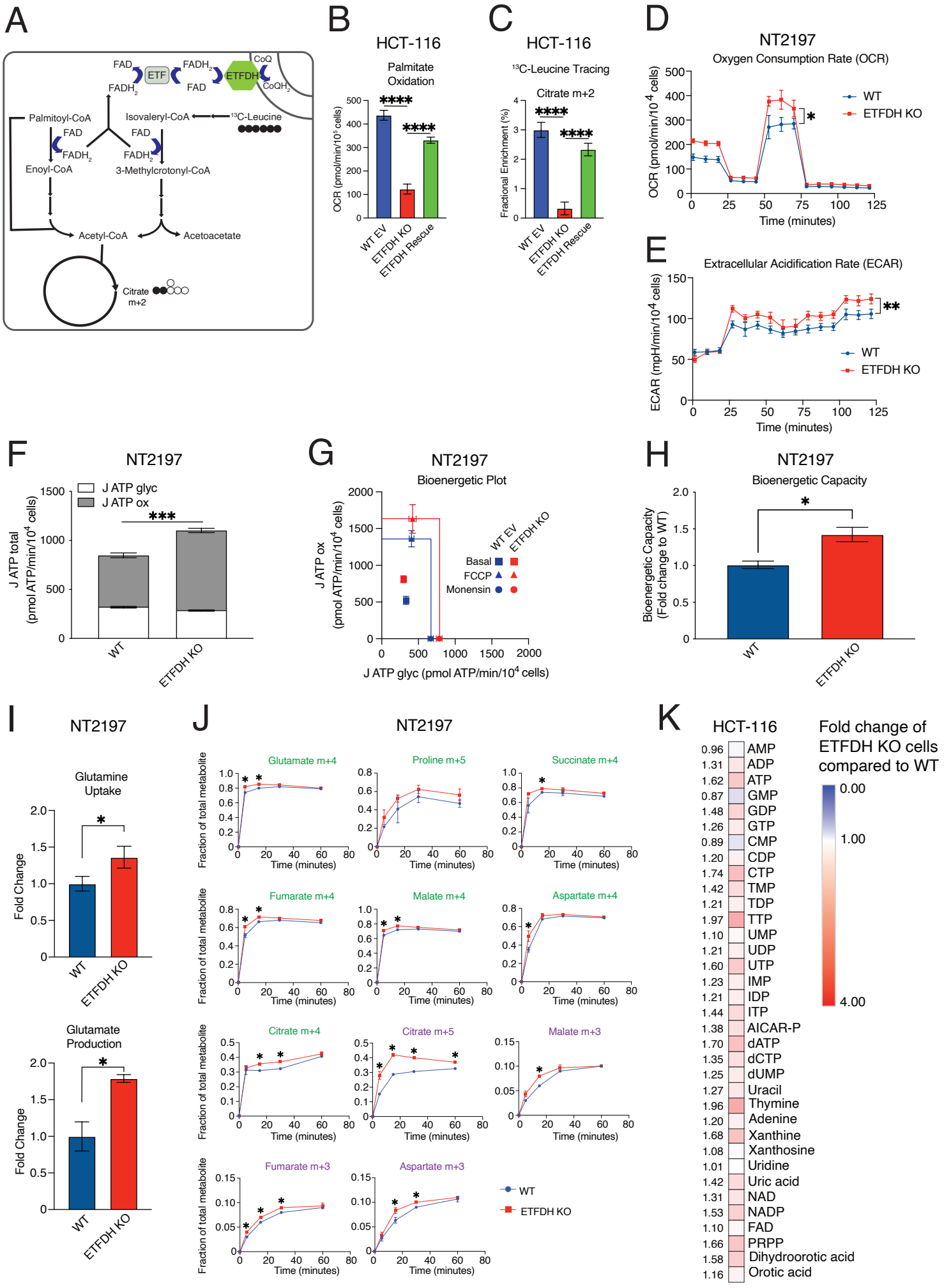

Supplementary Figure 3

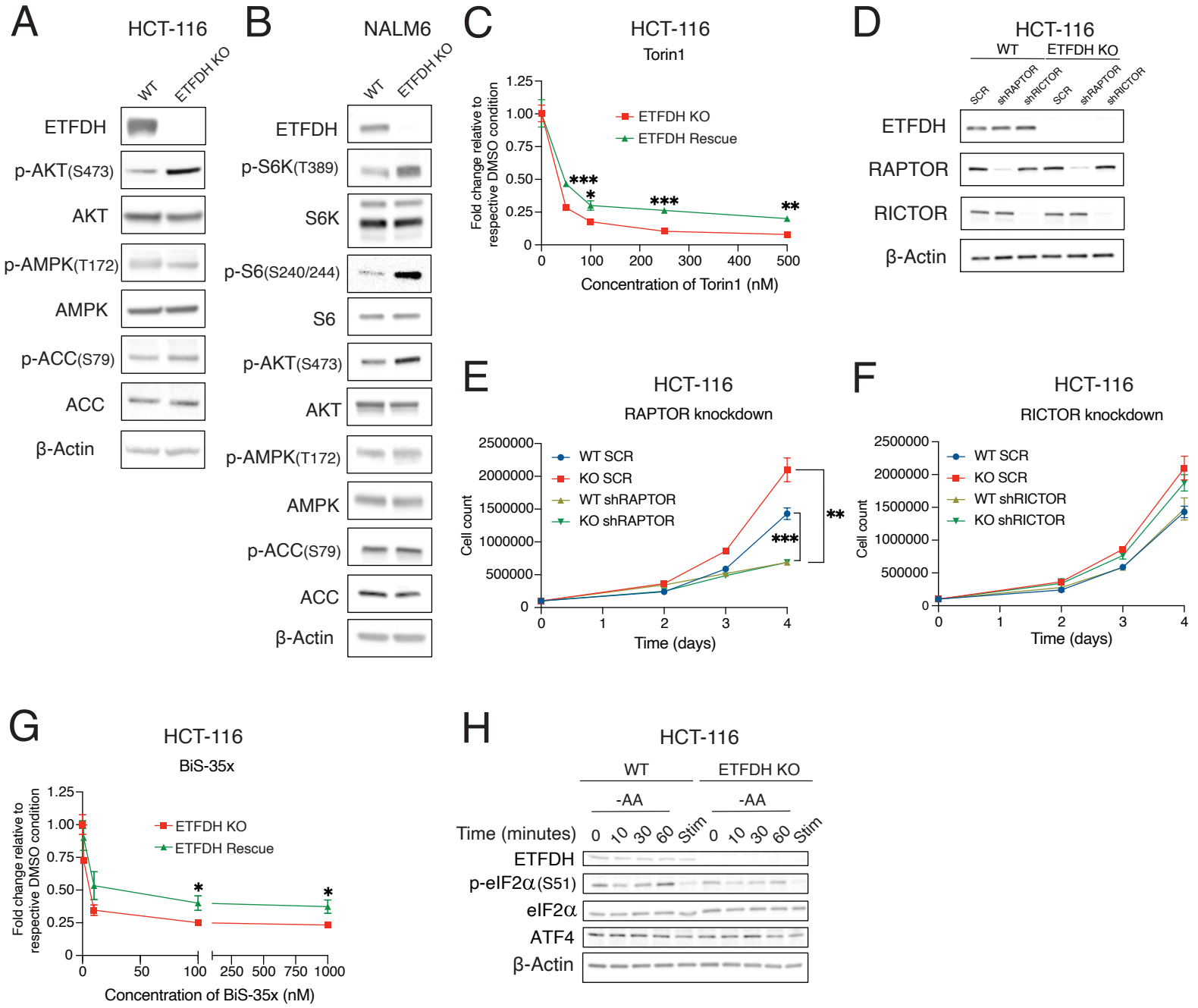

Supplementary Figure 4

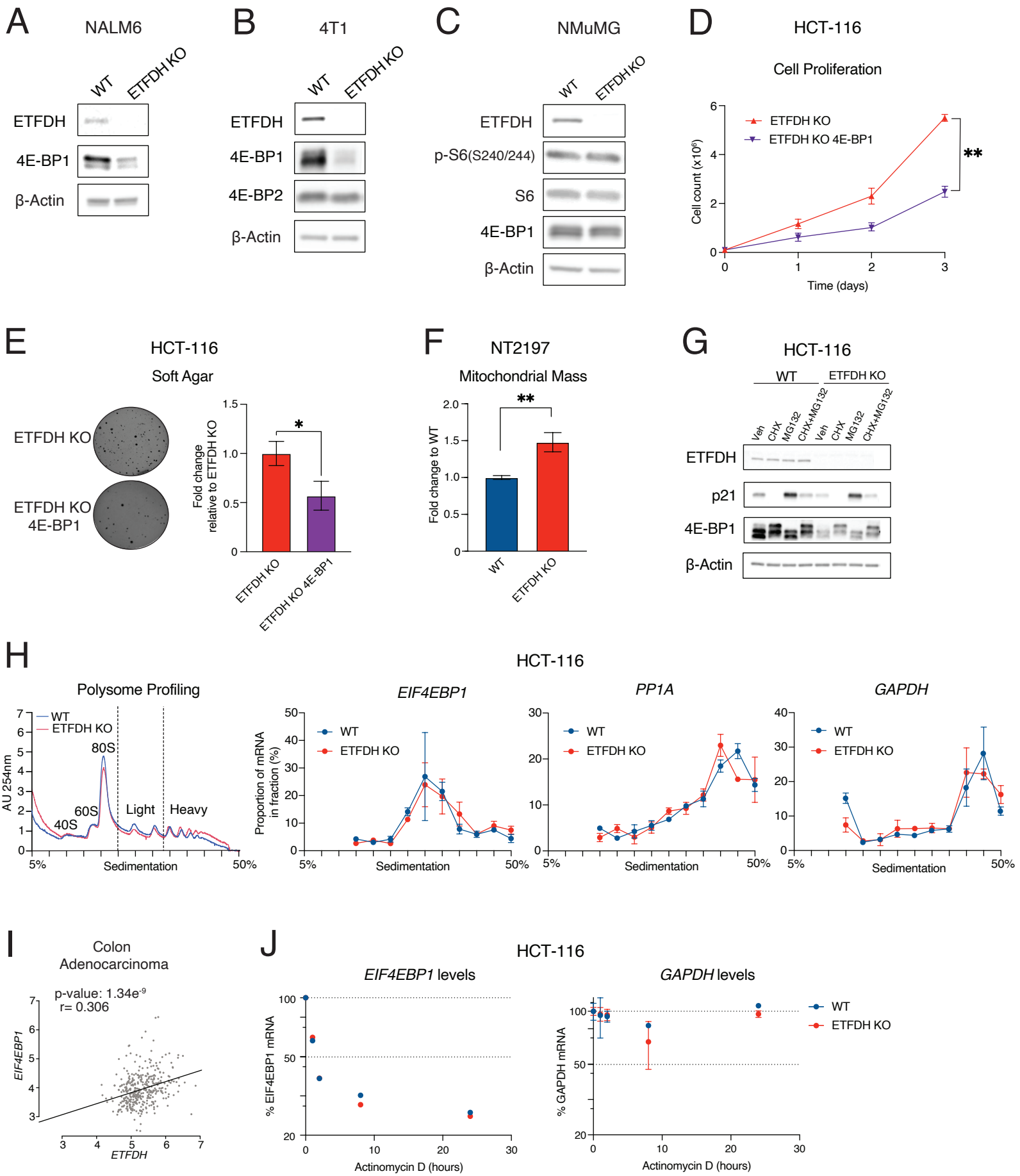

Supplementary Figure 5

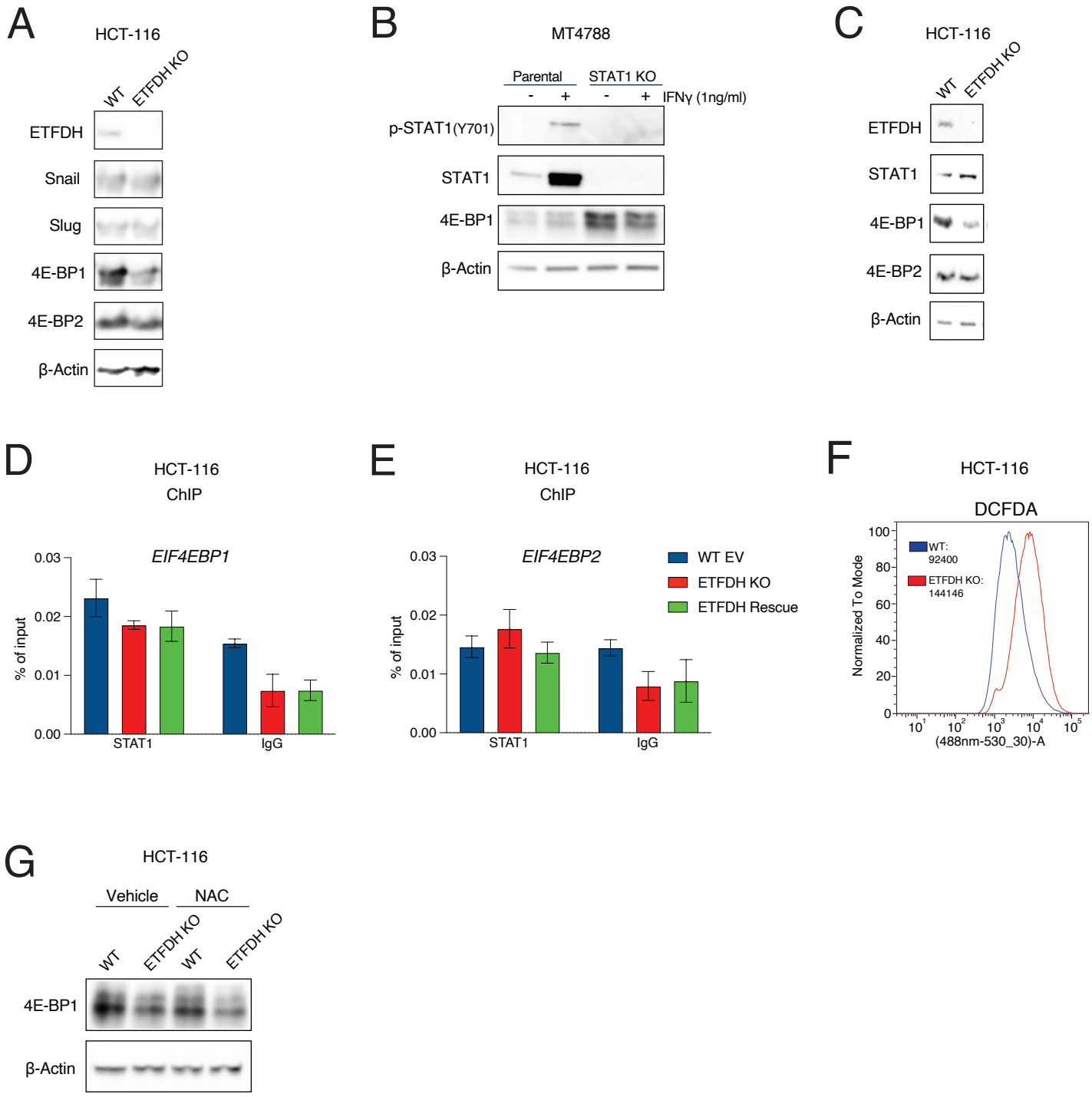

Supplementary Figure 6

A

```
                1                                                                                                                                                                                                                                                                                                                                                                                                                                                                                                                                                                                                                                                                                                                                                                                                                                                                                                                                                                                                                                                                                                                                                                                                                                                                                                                                                                                                                                                                                                                                                                                                                                                                                                                                                                                                                                                                                                                                                                                                                                                                                                                                                                                                                                                                                                                                                                                                                                                                                                                                                                                                                                                                                                                                                                                                                                                                                                                                                                                                                                                                                                                                                                                                                                                                                                                                                                                                                                                                                                                                                                                                                                                                                                                                                                                                                                                                                                                                                                                                                                                                                                                                                                                                                                                                                                                                                                                                                                                                                                                                                                                                                                                                                                                                                                                                                                                                                                                                                                                                                                                                                                                                                                                                                                                                                                                                                                                                                                                                                                                                                                                                                                                                                                                                                                                                                                                                                                                                                                                                                                                                                                                                                                                                                                                                                                                                                                                                                                                                                                                                                                                                                                                                                                                                                                                                                                                                                                                                                                                                                                                                                                                                                                                                                                                                                                                                                                                                                                                                                                                                                                                                                                                                                                                                                                                                                                                                                                                                                                                                                                                                                                                                                                                                                                                                                                                                                                                                                                
                172
WT Etfdh   ATGTTGGTGCGACTAACCAAGCTGTCCTGCCCTGCGTATCACTGGTTTCATGCCTTAAAAATTAAGAAGTGCCTACCTCTGTGTGCTCCAAGATGTTCTTCAACCTCTGCTGTA————————————————CCTCAGATTACCACTCACTACACTGTTCATCCCCGGGAGA....
(AAG)6     ATGTTGGTGCGACTAACCAAGCTGTCCTGCCCTGCGTATCACTGGTTTCATGCCTTAAAAATTAAGAAGTGCCTACCTCTGTGTGCTCCAAGATGTTCTTCAACCTCTGCTGTAAAGAAGAAGAAGAAGAAGCCTCAGATTACCACTCACTACACTGTTCATCCCCGGGAGA....
(AAA)4     ATGTTGGTGCGACTAACCAAGCTGTCCTGCCCTGCGTATCACTGGTTTCATGCCTTAAAAATTAAGAAGTGCCTACCTCTGTGTGCTCCAAGATGTTCTTCAACCTCTGCTGTAAAAAAAAAAAA————CCTCAGATTACCACTCACTACACTGTTCATCCCCGGGAGA....
(AAA)6     ATGTTGGTGCGACTAACCAAGCTGTCCTGCCCTGCGTATCACTGGTTTCATGCCTTAAAAATTAAGAAGTGCCTACCTCTGTGTGCTCCAAGATGTTCTTCAACCTCTGCTGTAAAAAAAAAAAAAAAAAACCTCAGATTACCACTCACTACACTGTTCATCCCCGGGAGA....
```

B

(AAG)6 / (AAA)6 Protein Structure

C

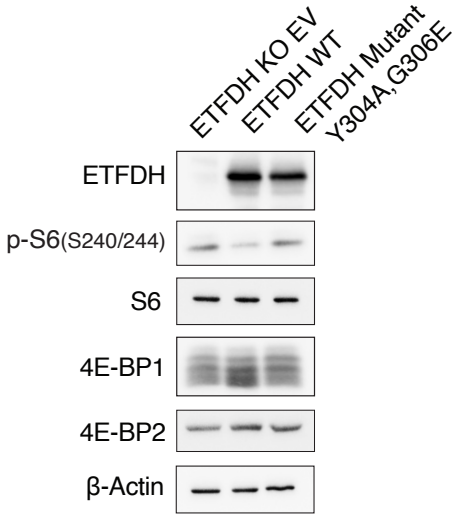

D

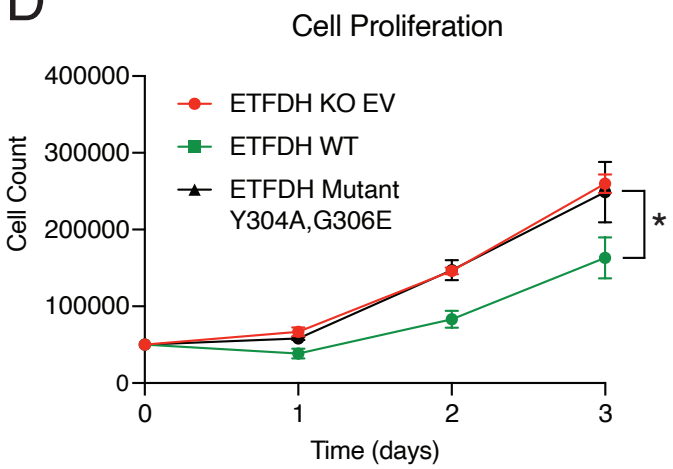

E

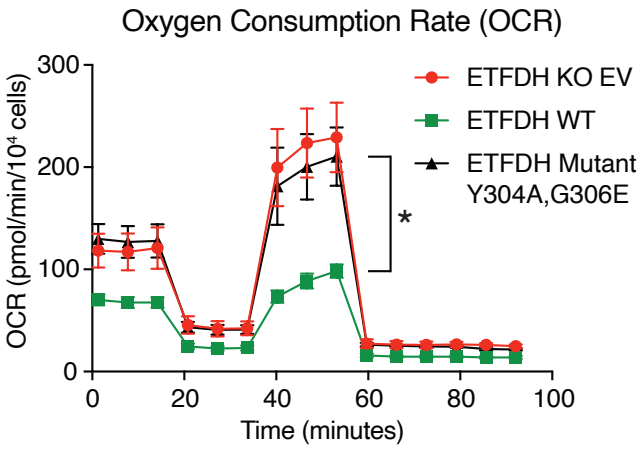

F

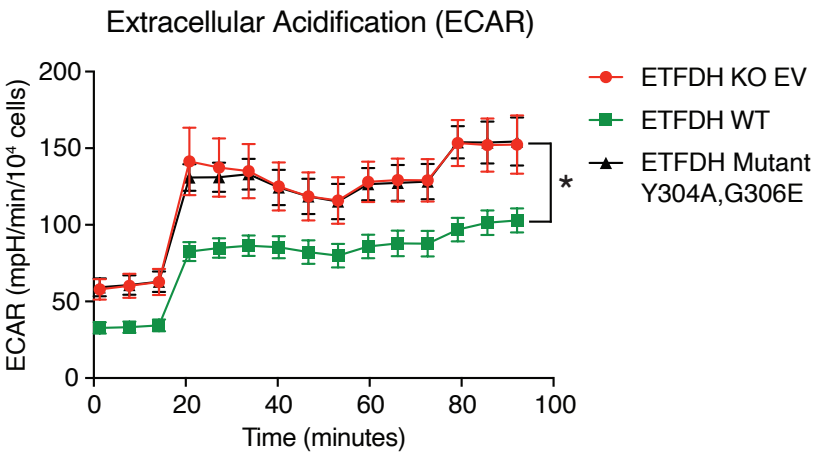

Supplementary Table 1 List of Antibodies

Antibody	Source	Identifier
Mouse monoclonal β-actin antibody, 1:5000 dilution	MilliporeSigma	Cat#A5441; RRID: AB_476744
Normal Rabbit IgG	Cell Signaling Technologies	Cat#2729; RRID: AB_1031062
Rabbit monoclonal 4E-BP1 (53H11) antibody, 1:1000 dilution	Cell Signaling Technologies	Cat#9644; RRID: AB_2097841
Rabbit monoclonal Akt (pan) (C67E7) antibody, 1:1000 dilution	Cell Signaling Technologies	Cat#4691; RRID: AB_915783
Rabbit monoclonal phospho-4E-BP1 (S65) (174A9) antibody, 1:1000 dilution	Cell Signaling Technologies	Cat#9456; RRID: AB_823413
Rabbit monoclonal Phospho-Akt (Ser473) (D9E) XP® antibody, 1:1000 dilution	Cell Signaling Technologies	Cat#4060; RRID: AB_2315049
Rabbit monoclonal Rictor (53A2) antibody, 1:1000 dilution	Cell Signaling Technologies	Cat#2114; RRID: AB_2179963
Rabbit polyclonal phospho-S6 Ribosomal Protein (Ser240/244) antibody, 1:2000 dilution	Cell Signaling Technologies	Cat#2215; RRID: AB_2630325
Rabbit polyclonal Raptor antibody, 1:1000 dilution	MilliporeSigma	Cat#09–217; RRID: AB_612103
Rabbit polyclonal 4E-BP2 antibody, 1:1000 dilution	Cell Signaling Technology	2845; RRID: AB_10699019
Rabbit monoclonal phospho-S6K (T389) antibody, 1:500 dilution	Cell Signaling Technology	9234; RRID: AB_2269803
Rabbit monoclonal S6K antibody, 1:1000 dilution	Cell Signaling Technology	2708; RRID: AB_390722
Mouse monoclonal S6 ribosomal protein antibody, 1:5000 dilution	Santa Cruz Biotechnology	sc-74459; RRID: AB_1129205
Rabbit polyclonal ACC antibody, 1:1000 dilution	Cell Signaling Technology	3662; RRID: AB_2219400
Rabbit polyclonal phospho-ACC (Ser79) antibody, 1:1000 dilution	Cell Signaling Technology	3661; RRID: AB_330337
Mouse monoclonal eIF2α (L57A5) antibody, 1:1000 dilution	Cell Signaling Technology	2103; RRID: AB_836874
Rabbit polyclonal eIF2α (Ser51) antibody, 1:1000 dilution	Cell Signaling Technology	9721; RRID: AB_330951
Rabbit polyclonal eIF4G1 antibody, 1:500 dilution	Cell Signaling Technology	2858; RRID: AB_2095745
Rabbit polyclonal TFAM antibody, 1:1000 dilution	Cell Signaling Technology	7495; RRID: AB_10841294
Rabbit monoclonal GAPDH (14C10) antibody, 1:1000 dilution	Cell Signaling Technology	2118; RRID: AB_561053
Mouse monoclonal eIF4E antibody, 1:1000 dilution	BD Biosciences	610269; RRID: AB_397664
Mouse monoclonal puromycin (12D10) antibody, 1:1000 dilution	Millipore	MABE343; RRID: AB_2566826
Rabbit polyclonal AMPKα antibody, 1:500 dilution	Cell Signaling Technology	2532; RRID AB_330331
Rabbit monoclonal Anti-AMPK-alpha, phospho (Thr172) antibody, 1:500 dilution	Cell Signaling Technology	2535; RRID: AB_331250
Rabbit polyclonal ETFDH antibody, 1:2000 dilution	ProteinTech	11109-1-AP; RRID: AB_2231382
Rabbit monoclonal BCL-6 antibody, 1:1000 dilution	Cell Signaling Technology	14895; RRID: AB_2798638
Rabbit monoclonal BCL-6 antibody, 1:1000 dilution	Cell Signaling Technology	5650; RRID: AB_10949970
Rabbit monoclonal Snail antibody, 1:1000 dilution	Cell Signaling Technology	3879; RRID: AB_2255011
Rabbit monoclonal Slug antibody, 1:1000 dilution	Cell Signaling Technology	9585; RRID: AB_2239535
Rabbit polyclonal CREB-2 (ATF4) antibody, 1:1000 dilution	Santa Cruz	sc-200; RRID: AB_2058752
Rabbit monoclonal STAT1 antibody, 1:1000 dilution	Cell Signaling Technology	14994; RRID: AB_2737027
Rabbit monoclonal p-STAT1 (Tyr701) antibody, 1:1000 dilution	Cell Signaling Technology	9167; RRID: AB_561284

Supplementary Table 2: Primer sequences used for RT-qPCR

Primer Name	Primer Sequence
Human	
EIF4EBP1 forward	GGAACTCACCTGTGACCAAAA
EIF4EBP1 reverse	CCGCTTATCTTCTGGGCTATT
EIF4EBP2 forward	AGTCACTAGCCCTGGCACCTTA
EIF4EBP2 reverse	CTTGCAGGAGAGTCAGATGTCC
BCL6 forward	TGAGAAGCCCTATCCCTGTG
BCL6 reverse	TGTGACGGAAATGCAGGTTA
PP1A forward	GTCAACCCCACCGTGTTCTT
PP1A reverse	CTGCTGTCTTTGGGACCTTGT
GAPDH forward	TGTTGCCATCAATGACCCCTT
GAPDH reverse	CTCCACGACGTACTCAGCG
Mouse	
Eif4ebp1 forward	GGTCACTAGCCCTACCAGCG
Eif4ebp1 reverse	TTGTGACTCTTCACCGCCTG
Eif4ebp2 forward	TACCTCAGGACTACTGCACCAC
Eif4ebp2 reverse	GGAGAATTGCGACGGTCCAACA
Bcl6 forward	GCGAACCTTGATCTCCAGTC
Bcl6 reverse	TGACTCTCACTGCTGCTTCG
Actb forward	TTCCTTCTTGGGTATGGAA
Actb reverse	CCACGATCCACACAGAGTA

Supplementary Table 3: Primer sequences used for ChIP-qPCR

Primer Name	Primer Sequence
EIF4EBP1_ChIP forward	TGACTGAGGTTCGGATCTGG
EIF4EBP1_ChIP reverse	CACTCGCGTAAATGGGGAAC
EIF4EBP2_ChIP forward	TTCAACAACTTCAGCCACGC
EIF4EBP2_ChIP reverse	GGAGTTGGGGAAGCTGGTC

Supplementary Table 4: gRNA sequences used for generation of ETFDH KO cell lines

Primer Name	Primer Sequence
Human	
ETFDH gRNA Target 1 Forward	CACCGAGGTTGGCCGAATGCTAGGA
ETFDH gRNA Target 1 Reverse	AAACTCCTAGCATTCGGCCAACCTC
ETFDH gRNA Target 2 Forward	CACCGATGTAGGGATACAAAAGGA
ETFDH gRNA Target 2 Reverse	AAACTCCTTTTGTATCCCTACATC
Mouse	
ETFDH gRNA Target 1 Forward	CACCGGTGATACGCTGCATAAAAAT
ETFDH gRNA Target 1 Reverse	AAACATTTTTATGCAGCGTATCACC
ETFDH gRNA Target 2 Forward	CACCGGAACATCTTGGAGCACACAG
ETFDH gRNA Target 2 Reverse	AAACCTGTGTGCTCCAAGATGTTCC

Supplementary Table 5: Primer sequences used for sequencing

Primer Name	Primer Sequence
Human	
ETFDH validation Set 1 Forward	AGCGAGCATTTTCCTCCACA
ETFDH validation Set 1 Reverse	ACCATTGTTAGCTCAAAGTTGCT
ETFDH validation Set 2 Forward	TCATTTCCCATTGTGCGAGC
ETFDH validation Set 2 Reverse	ATGTACAGTTTGTAGCAAGACCT
Mouse	
ETFDH validation Set 1 Forward	GTGTCTGAAGGCAGCAACAG
ETFDH validation Set 1 Reverse	GGATCAAGACAAGCCCCTGA
ETFDH validation Set 2 Forward	CCAGGTTCAATTCCCAGCAC
ETFDH validation Set 2 Reverse	CCGGGGATGAACAGTGTAGT